University of Nevada, Reno

Characterization Emissions from Open Combustion of Cheatgrass (*Bromus Tectorum*)

A thesis submitted in partial fulfillment of the requirements for the degree of Master of Science in Atmospheric Science

by

Megan J. Rennie

Dr. Hans Moosmüller/Thesis Advisor

December, 2019

THE GRADUATE SCHOOL

We recommend that the thesis
prepared under our supervision by

MEGAN RENNIE

Entitled

Characterization Emissions from Open Combustion of Cheatgrass (Bromus Tectorum)

be accepted in partial fulfillment of the
requirements for the degree of

Master of Science

Hans Moosmüller, Ph.D., Advisor

W. Patrick Arnott, Ph.D., Committee Member

Vera Samburova, Ph.D., Graduate School Representative

David W. Zeh, Ph.D., Dean, Graduate School

December, 2019

Abstract

Cheatgrass (*Bromus Tectorum*) is a highly invasive species dominant in the Great Basin of the Western United States. Early spring growth combined with early summer drying supplies large amounts of highly flammable fuel to sagebrush and other ecosystems increasing the frequency and intensity of wildland fires. Despite the importance of cheatgrass for the fire ecology of large parts of the western U.S., emission factors (EF) for its combustion are largely unknown. The fresh smoke from 12 open laboratory burns of cheatgrass has been analyzed using real-time measurements. Here, we present measured optical properties, absorption Ångström exponents (AAE), scattering Ångström exponents (SAE), and the single scattering albedos (SSA) of the emitted smoke. We also quantify gaseous elemental mercury (GEM) emission factors from the laboratory combustion of cheatgrass and show that cheatgrass EFs are comparable to those of other grasses.

Dedication

I would like to dedicate this thesis to my husband, Joshua Rennie. I will always appreciate your support throughout my schooling and late-night research hours and your willingness to collect cheatgrass in the summer heat without hesitation. Thank you for always being my biggest supporter.

Acknowledgments

I wish to deeply thank my committee members who graciously shared their time and knowledge with me in my pursuit of education. A special thanks to my advisor Dr. Hans Moosmüller, your willingness to share your knowledge and experience with me while allowing me to test the waters of laboratory research and pursue education beyond the bounds of a classroom has been invaluable to me. Thank you to Dr. Vera Samburova and Dr. W. Patrick Arnott. You have each left a lasting impression on both my work and my education.

Thank you to my coauthors, Dr. Daniel Obrist and Andrey Khlystov, for your time, hard work, and expertise. I would like to acknowledge the Desert Research Institute for allowing me to conduct research in an environment that supports continuing expansion of knowledge through research. To the International Wildland Fire Association, thank you for your support, it has been an honor to receive such great recognition of my research through your scholarship.

Finally, I would like to thank the ardent faculty at the University of Nevada, Reno who imparted excitement and passion for my education.

Table of Contents

List of Tables

List of Figures

Introduction

Wildland fires are changing resources throughout the Great Basin while increasing noxious weeds and exotic annual grasses, thereby creating more dangerous and costly wildland fires. Invasive cheatgrass has increased the frequency and extent of rangeland fires ten-fold (Bradley et al. 2006) by creating higher fuel loads and dense vegetative coverage in areas where shrubs and desert grasses were once separated by open areas of soil. Cheatgrass typically germinates in the fall, continues root growth throughout winter months, initiates growth in early spring, and has a higher growth rate compared to native plants. Cheatgrass becomes highly competitive for water and dries by early summer supplying large amounts of highly flammable fuel that connects shrubland areas during fire propagation that were once separated, thereby facilitating an earlier fire season.

More frequent wildland fires are changing the landscape ecology in the US Intermountain West (USIMW), a region that covers Nevada, Utah, Idaho, parts of Arizona, and western Colorado (Bradley et al. 2018), while ironically changing the nature of wildland fires. Sagebrush can withstand fire frequencies on the scale of decades yet cheatgrass is an annual plant with seeds that can withstand yearly wildfires. Cheatgrass invasion can convert ecosystems that are at high risk for conversion to annual grasslands (Bradley et al. 2006) from a carbon sink to a carbon source with a potential emission of 50 ± 20 Tg C over the next 60 years in dry desert shrub areas. Emissions from wildland fires contribute to air pollution events, affect the radiative budget and climate change, and can cause severe health effects (Martinsson et al. 2015; 2016; Stocks et al. 1998).

Characterizing the optical properties of aerosols emitted from the open combustion of cheatgrass (*Bromus Tectorum*), an exotic annual grass species in the USIMW, will help develop an understanding of the role that smoke from cheatgrass wildland fires plays in changing the regional energy budget. The absorption of solar radiation by aerosols emitted during combustion of cheatgrass heats these particles and consequently the surrounding atmosphere, reducing the amount of solar radiation that reaches the surface, thereby affecting planetary albedo, atmospheric stability, and cloud processes. The smoke from cheatgrass wildfires is a source of carbonaceous aerosols and my research is helping to understand and mitigate their influence on radiative forcing and to improve their remote sensing. The emission factors (EFs) for and properties of aerosols emitted from sagebrush combustion have previously been characterized McMeeking et al. (2009), but emissions from cheatgrass combustion have not. This results in increased uncertainties for wildland fire emissions in the USIMW as cheatgrass continues to spread. Cheatgrass burns primarily in the flaming phase of combustion where large amounts of black carbon are emitted. Laboratory burns were performed to quantify EFs for physical and chemical properties of cheatgrass combustion emissions including the emission of gaseous elemental mercury (GEM). In chapter 1, I will discuss the measurement and calculations of EFs, optical properties: absorption Ångström exponents (AAE), scattering Ångström exponents (SAE), and the single scattering albedos (SSA) of the emitted smoke, along with combustion properties. In chapter 2, I will present the EF of gaseous elemental mercury (GEM) and present a comparison to previously reported EFs from laboratory experiments, wildfire plumes, and laboratory measurements of grasslands, savannahs, and sagebrush.

Chapter 1
Emissions from the Open Laboratory Combustion of Cheatgrass (*Bromus Tectorum*)

M. Rennie[1,2]*, V. Samburova[1,2], W. P. Arnott[2], A. Khlystov[1], H. Moosmüller[1]
[1]Division of Atmospheric Sciences, Desert Research Institute, Reno, NV, USA
[2] University of Nevada-Reno, Reno, NV, USA

Abstract

Cheatgrass (*Bromus Tectorum*) is a highly invasive species in the Great Basin that is increasing the frequency and intensity of wildland fires. The fresh smoke from 12 open laboratory burns of cheatgrass have been analyzed using real-time measurements. We present the measured intensive optical properties of the emitted smoke; absorption Ångström exponents (AAE), scattering Ångström exponents (SAE), and the single scattering albedos (SSA). We are also discussing the modified combustion efficiency and the fuel-based emission factors (EF) of cheatgrass along with a comparison to previously reported EFs of similar fuels.

Introduction

Cheatgrass (*Bromus Tectorum*) is an invasive grass that has extensive ecological impacts (Bradley et al. 2018) and is rapidly spreading through the sagebrush ecosystem of the Great Basin (Bradley et al. 2018) that covers most of Nevada, much of Utah, and smaller portions of Oregon, California, Idaho and Wyoming, USA. This invasion results in new uncertainties for wildland fire emissions in the Great Basin. Specifically, emission factors (EFs) for and properties of aerosols emitted from sagebrush combustion have been characterized McMeeking et al. (2009), but emissions from cheatgrass combustion have not. Furthermore, cheatgrass is increasing the frequency and magnitude of rangeland fires ten-fold (Bradley et al. 2006) by creating higher fuel loads and higher vegetative coverage

in areas where shrubs and desert grasses were once separated by open areas of soil. Regions where spatial cheatgrass coverage reaches more than 15%, are more than twice as likely to experience a wildland fire compared to regions where the cheatgrass coverage is minimal (Bradley et al. 2018). The increased fine fuel accumulation also increases the likelihood of the destruction of native plants during wildland fire events (Davies & Nafus, 2013). Cheatgrass is rapidly invading much of the Great Basin, causing additional carbon emissions (Urbanski et al. 2018) through increased fire frequency in rangelands (Dantonio & Vitousek, 1992).

Our study of cheatgrass combustion emissions was conducted with cheatgrass harvested from a site near Reno, Nevada that had most recently burned during the Hawken fire in June 2016. This fire burned through native vegetation destroying most sagebrush and other chaparral plants which allows for increased cheatgrass growth in the area. On average, Reno, NV. USA receives 300 days of sunshine and ~20 cm of precipitation per year and is considered a cold desert climate. The area around Reno, NV is dominated by a sagebrush ecosystem where cheatgrass is most invasive and persistent. Cheatgrass burns primarily in the flaming combustion phase, where a diffusion flame burns emitted volatiles, in the process emitting large amounts of black carbon (BC) particles and trace gases into the atmosphere (Chen et al. 2007; McMeeking et al. 2009). Flaming combustion is the most common combustion phase for biomass burning of low-fuel-moisture foliage and grasses. This combustion also emits most BC mass and thereby increases the light absorption of smoke (Satheesh & Moorthy, 2005). Flaming combustion is often followed by smoldering

combustion, where low temperature oxidation of solid fuels takes place, emitting large amounts of carbon monoxide (CO) and organic carbon (OC) (Rein, 2016).

Emissions of polycyclic aromatic hydrocarbons (PAHs) from the open combustion of cheatgrass have previously been reported by Samburova et al., (2016), but otherwise, very little is known about cheatgrass combustion emissions. Here, we measured the modified combustion efficiency (MCE) which is the ratio of CO_2 to $CO+CO_2$ that is used to determine whether a burn is dominated by flaming or smoldering combustion. Selimovic et al. (2018) found that the ratio of brown carbon (BrC) absorption to black carbon (BC) absorption is highly dependent of the MCE. BrC is a light-absorbing organic carbon that strongly absorbs in the ultra-violet (UV) wavelengths (Lewis et al. 2008).

We have also measured smoke optical properties and fuel-based emission factors (EFs), which, to the best of our knowledge have not been reported previously. We are reporting on values measured from 2019 as well as EFs from a previous 2014 biomass burning experiment. Optical properties reported include SSA, an intensive aerosol property that equals the ratio of scattering to extinction coefficient and is essential for determination of aerosol radiative forcing (Chylek & Wong, 1995; Hassan, Moosmüller, & Chung, 2015), absorption Ångström exponents (AAE), and scattering Ångström exponents (SAE), characterizing the wavelength dependence of aerosol absorption and scattering coefficients, respectively (Moosmüller & Chakrabarty, 2011).

Methods and Data:

Experiment details and setup:

Starting in June and continuing through September, cheatgrass fuel samples were collected monthly from 39°28’58” N, 119°51’57” W at 1517 m of elevation. This site is located in the western foothills of the Reno, NV, USA valley inside the Hawken fire burn scar. Vegetation samples were collected using clean latex gloves and clean Zip-lock bags to avoid contamination. The biomass burning experiments took place in the biomass combustion facility of the Desert Research Institute (DRI). A detailed description of a close replicate of this chamber has been given by Tian et al. (2015). The facility consists of sealable chamber (1.8 m x 1.8 m x 2.0 m) with aluminum walls that taper at the roof, funneling smoke into an exhaust pipe. Combustion exhaust is sampled from this pipe through copper tubes and provided to instrumentation for real-time and filter sampling. The chamber flow rate is controlled by a fan in the exhaust pipe and by a gate controlling the air inlet, located underneath the chamber.

For our combustion experiments, the fan was turned off and the gate was fully closed allowing combustion emissions to accumulate within the chamber, similar to the methods used by McMeeking et al. (2009). Cheatgrass was piled on top of a continuously weighed ceramic disk in the chamber to monitor fuel mass loss during the burning period. The copper pipe that connected the chamber to the real-time sampling instruments was disconnected and the fuel was ignited with a butane lighter. The chamber was allowed to fill with smoke for 5 minutes to sample a uniform aerosol distribution in the chamber for ~ 5 minutes. At the end of this 5-minute time period, the chamber was reconnected to the

sampling line. The real-time instruments then measured smoke from the chamber until smoke dropped to near-ambient levels.

The instruments used to characterize emission factors (EF) and optical and physical aerosol properties consisted of a CO (Thermo 48i carbon monoxide analyzer, Waltham, MA, USA) and a CO_2 analyzer (Li-7000 CO2/H2O Analyzer, Lincoln, NE, USA), a three-wavelength photoacoustic soot spectrometer (PASS-3, Droplet Measurement Technologies, Boulder, CO, USA), and a Scanning Mobility Particle Sizer 3080 classifier (SMPS Shoreview, MN, USA).

Absorption (b_{abs} Mm^{-1}) and scattering (b_{scat} Mm^{-1}) coefficients were measured using the PASS-3 (Lewis et al. 2008). Particle mass concentrations and size distributions were measured with the SMPS, which consists of a TSI 3081 differential mobility analyzer (DMA) and TSI 3775-condensation particle counter (CPC). These instruments sampled an input flow of 1 l/min, reporting results every second except for the SMPS which sampled using a 3.0 l/min sheath flow through the DMA and a 0.3 l/min sample flow through the CPC. The CO_2 and CO monitors were checked for accuracy prior to each burn and calibration was performed, if needed. After collection, cheatgrass fuel samples were allowed to air dry at room temperature. Fuels were dried over night at 90°C and measured for mass loss to determine fuel moisture content (FMC). FMC ranged from 4% to 9% FMC.

Fuel Characteristic

Figure 1: Cheatgrass in Reno, NV, USA is turning from green to purple as the plants mature.

Cheatgrass is a plant native to Eurasia that has aggressively invaded North America with an ability to produce over 10,000 plants per square mile (Beck, 2012). Cheatgrass grows quickly in spring before native species develop and dies by early summer, thereby contributing large amounts of dry, fine fuels that are easily ignitable. The plant is recognizable by the drooping seed heads, as seen in Figure 1, and fine hairs covering the plant. The young plants are green, turning to purple, during further maturation, its color fades into a pale golden brown as the plant dies. Typical height of the plant is between 3- 30 inches and its seeds are covered with bristle-like hairs that allow for dispersion by wind or animal fur. Fuels and ashes from each burn were analyzed for total carbon, nitrogen, hydrogen, and oxygen mass content at the DRI's Environmental Analysis Facility (EAF).

Burn Emissions:

Modified combustion efficiency:

The modified combustion efficiency (MCE) approximates the fraction of emitted carbon that is in the form of CO_2 and depends on the fuel combustion (e.g., flaming vs. smoldering). MCE is calculated as the ratio of molar CO_2 and CO excess concentrations as

$$\mathrm{MCE} = \frac{\Delta[\mathrm{CO_2}]}{\Delta[\mathrm{CO_2}]+\Delta[\mathrm{CO}]} \quad (1)$$

where ΔCO_2 and ΔCO are the mixing ratios of CO_2 and CO with the background concentration subtracted, respectively. Here, the subtracted background concentrations were the mean of the concentrations measured in the chamber over the 2 minutes prior to the burn's ignition. The MCE is a qualitative indicator of the amount of flaming and smoldering combustion present since in a typical burn there is a mixture of both combustion phases. In flaming combustion, the reaction oxidizes C, N, H, and S and turns them into common greenhouse gases like CO_2, H_2O, NO_x, and SO_2 (Akagi et al. 2011) with a MCE of about 0.99 for pure flaming combustion (Urbanski 2013). The MCE of smoldering combustion ranges from 0.65 to 0.85 (Urbanski 2013). MCE is also related to the amounts of OC and BC emitted; flaming combustion emits more BC while smoldering combustion emits more OC and its component BrC.

Emission factors:

The fuel-based emission factor (EF_n) for a species, n, is the ratio of n mass concentration emitted (M_n) to dry fuel mass burned (M_{fuel}) as

$$EF_n = \frac{M_n}{M_{fuel}} = \frac{M_n}{M_C} * CMF_{fuel} = \frac{C_n}{C_C} * CMF_{fuel} = \frac{C_n}{\frac{12}{44}C_{CO_2} + \frac{12}{28}C_{CO}} * CMF_{fuel}, \quad (2)$$

where M_{fuel} was determined as the ratio of total carbon mass emitted (M_C) and the carbon mass fraction of the dry fuel (CMF_{fuel}) as

$$M_{fuel} = \frac{M_C}{CMF_{fuel}}, \quad (2b)$$

where the total carbon mass emitted (M_C) is well approximated by the sum of carbon mass in carbon dioxide ($M_{C_{CO_2}}$) and carbon monoxide ($M_{C_{CO}}$) as

$$M_C = M_{C_{CO_2}} + M_{C_{CO}} = \frac{12}{44}M_{C_{CO_2}} + \frac{12}{28}M_{CO}, \quad (2c)$$

In this equation we neglect the ash carbon content which is typically less than 5% of the fuel mass (Chen et al. 2007). The CMF_{fuel} was determined through fuel analysis with a Thermo Scientific™ EA 1112 Series CHNS-O Analyzer (Waltham, MA, USA) for total carbon, nitrogen, hydrogen, and oxygen ratios at the DRI's Environmental Analysis Facility (EAF). Emission factors for particulate matter (EF_{PM}) were calculated using the mass concentration measured with the SMPS. CO_2 and CO were measured from the LiCor and Thermo analyzers. Background concentrations were removed, and the excess of CO_2 and CO were used to calculate the EFs.

Optical properties

Single scattering albedo

Aerosol absorption (b_{abs}) and scattering (b_{scat}) coefficients were measured with the PASS-3 to calculate the single scattering albedo (SSA). SSA is an intensive property that equals the ratio of scattering efficiency to total extinction efficiency for an ensemble of particles as

$$SSA = \frac{b_{scat(\lambda)}}{b_{scat(\lambda)}+b_{abs(\lambda)}} = \frac{b_{scat(\lambda)}}{b_{ext(\lambda)}}, \quad (3)$$

where b_{scat} is the light-scattering coefficient (Mm^{-1}), b_{abs} is the light-absorption coefficient (Mm^{-1}), and λ is the wavelength of light (Moosmüller & Sorensen, 2018a, 2018b). The term b_{ext}, the extinction coefficient, is the sum of the scattering and absorption coefficients. The aerosol SSA influences radiative fluxes and heating in the atmosphere. Mostly absorbing aerosols (SSA ≈ 0) have a heating effect while mostly scattering ones

(SSA ≈ 1) have a cooling effect (Moosmüller, Chakrabarty, & Arnott, 2009; Moosmüller et al. 2012).

Absorption Ångström Exponent

The absorption Ångström exponent (AAE) is an intensive aerosol optical property describing the wavelength dependence of the aerosol absorption coefficient. AAE has also been used quantitatively to separate brown carbon (BrC) absorption from black carbon (BC) absorption. BC is highly absorbing in the visible and near-visible spectrum while BrC is highly absorbing in the near-UV and blue-spectrum. AAE is the negative slope of a log/log plot of the absorption coefficient as a function of wavelength and can be written as

$$\mathrm{AAE} = -\frac{(\ln(b_{abs}(\lambda_1) - \ln(b_{abs}(\lambda_2))}{(\ln(\lambda_1) - \ln(\lambda_2))}, \quad (4)$$

where b_{abs} is the wavelength dependent absorption coefficient. AAE is calculated from two b_{abs} coefficients measured by the PASS-3 at two different wavelengths. AAE values much larger than one are typical for aerosols emitted by smoldering biomass burning and are caused by BrC absorption. AAE values of about 1 typically indicate absorption from BC (Moosmüller et al. 2009).

Scattering Ångström Exponent

The scattering Ångström exponent (SAE) characterizes the wavelength dependence of aerosol light scattering. SAE depends on the dominant size mode of a mixture of aerosols, and combined with the AAE it can give insight into the nature of the aerosol (Pistone et al. 2019). The value of the SAE, which is the negative slope of the scattering coefficient as a function of wavelength on a log/log plot is

$$\mathrm{SAE} = -\frac{(\ln(b_{scatt}(\lambda_1) - \ln(b_{scatt}(\lambda_2))}{(\ln(\lambda_1) - \ln(\lambda_2))} \quad (5)$$

where b_{scat} is the wavelength dependent scattering coefficient.

Results and Discussion

Modified Combustion Efficiency

When ignited, cheatgrass burns rapidly and the flaming combustion phase dominates the carbon emission. Cheatgrass MCE for fuel harvested in different months ranged from 0.93 to 0.96 showing cheatgrass combustion is dominated by flaming combustion as is typical for dry, fine fuels. The MCEs reported in Table (1) are the average emission ratios for the first 5 minutes of the burn. Burns ignited quickly and caused an initially large increase in CO_2 concentrations followed by an increase in CO concentrations. The samples of cheatgrass harvested and burned in September experienced the shortest time from ignition to flames extinguishment (under 20 seconds) and along with August samples showed somewhat more smoldering combustion. However, differences in the MCE between monthly fuel samples were not statistically significant and the average MCE was 0.95±0.01. This MCE measured for cheatgrass is in good agreement with previously published MCE values reported for a prescribed grassland burn by (Urbanski, 2014) and for Dambo grass and Montana grass by (Chen et al. 2007).

	MCE	St.dev	Range	MCE	
June	0.96	0.03	0.92-0.98	Prescribed Fire Grassland[1]	0.947
July	0.95	0.03	0.92-0.97	Dambo Grass[2]	0.98±0.00
August	0.93	0.04	0.90-0.97	Montana Grass[2]	0.98-0.97
September	0.96	0.01	0.95-0.97	Savanna and grasslands[3]	0.94±0.02
Average	0.95	0.01			

Table 1: The monthly MCE was averaged over the first 5 minutes of the burn. On the right, previously reported data from a prescribed grassland fire Urbanski (2014),[1] open laboratory combustion of Dambo and Montana grass Chen et al. (2007) [2] (Andreae, 2019)[3] are in good agreement with our MCE values for cheatgrass.

Single Scattering Albedo (SSA)

The SSA, figure 2, is the ratio of scattering efficiency to total extinction efficiency. At the 405 nm wavelength, the SSA is lowest with a ranges of 0.81-0.85; here a significant part of the extinction (i.e. 15-19%) is due to absorption. The SSA at 405 nm has the least variation between the burns; it is indicative of the absorption of BrC which is highly absorbing in the UV. There is minimal variation in the SSA between the months, except for slightly lower SSA for the September fuel at the 532 nm and 781 nm wavelengths; here the fuel combustion emitted more BC, which is highly absorbing in the visible spectrum (Martinsson et al. 2015).

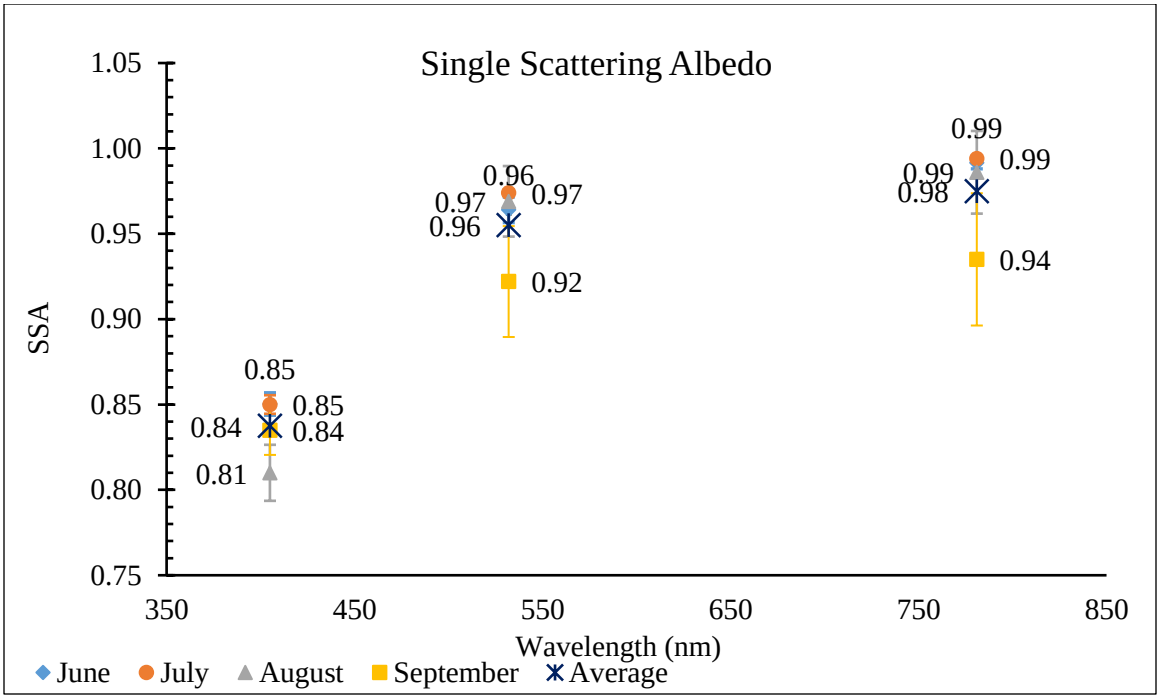

λ (nm)	405	532	781
June	0.85±(0.01)	0.96±(0.01)	0.99±(0.00)
July	0.85±(0.10)	0.97±(0.00)	0.99±(0.00)
August	0.81±(0.02)	0.97±(0.00)	0.99±(0.01)
September	0.84±(0.01)	0.92±(0.03)	0.94±(0.04)
Average	0.83±(0.02)	0.96±(0.02)	0.98±(0.03)

Figure 2: SSA at 405 nm, 532 nm, and 781 nm. The error bars seen in the graph above are the standard error.

Absorption and Scattering Coefficients Measured with the PASS-3

The PASS-3 utilizes the photoacoustic method to measure the light absorption by aerosols and integrated nephelometry to measure light scattering at the wavelengths of 405 nm, 532 nm, and 781 nm. Once a burn was lit and the chamber allowed to fill with smoke, the copper pipe was attached to the instrumentation and sampling began. The smoke was pulled into the PASS-3. Thick smoke lead to very high concentrations of particles. The absorption and scattering coefficients measured were the highest values that the PASS-3 had encountered in its usage at DRI. Smoke particles would be deposited onto the resonator windows, creating potential issues for future burns. In addition, during sampling, the

subtracted scattering background increased in time and the scattering coefficient would become saturated. Each month, three sample burns were performed and are denoted by A, B, and C.

Photoacoustic Saturation

During the combustion experiments, the exhaust fan was turned off and the air inlet gate was closed. The experiments followed this process with the concept that emissions would accumulate over time, resulting in near constant concentrations toward the end of the burn, but it resulted in an overloading of the PASS-3 photomultiplier tube (PMT) detector. In order to measure the aerosol scattering coefficient, the PASS-3 uses a PMT which detects light through the external photoelectric effect when an incident photon strikes a photocathode releasing an electron. The tube then amplifies the electrons using an electron multiplier directed by a focusing electrode.

Sampling of the chamber without air flow created a very high aerosol concentration that led to oversaturation of the PASS-3 PMT. The scattering coefficients behaved erratically once the PMT was saturated and the signal was greatly affected by the excess amplification of electrons generated. In figure 3, the behavior of the PMT becomes erratic once the 405 nm wavelength reaches a scattering coefficient of 500,000 Mm^{-1} or 0.5 m^{-1} is exceeded. In order to report meaningful optical properties, values of AAE and SAE are only reported before threshold limit. Values of AAE or SAE using coefficients above this threshold were deemed invalid and will note the scattering coefficient.

September Burn A

The first burn of fuel from September's collection is an example of a burn where saturation of the PMT occurred rapidly. September (Burn A) reached the threshold limit within the first minute of the sampling time. The PMT was greatly overloaded, and its signal takes an unknown time for recovery. As shown in figure 3, the 405 nm and 782 nm scattering signals quickly saturate with the second peak being greatly affected and measured scattering coefficients become meaningless. At the 532 nm wavelength, once saturation was initially reached the data became compromised and it took an unknown time for recovery.

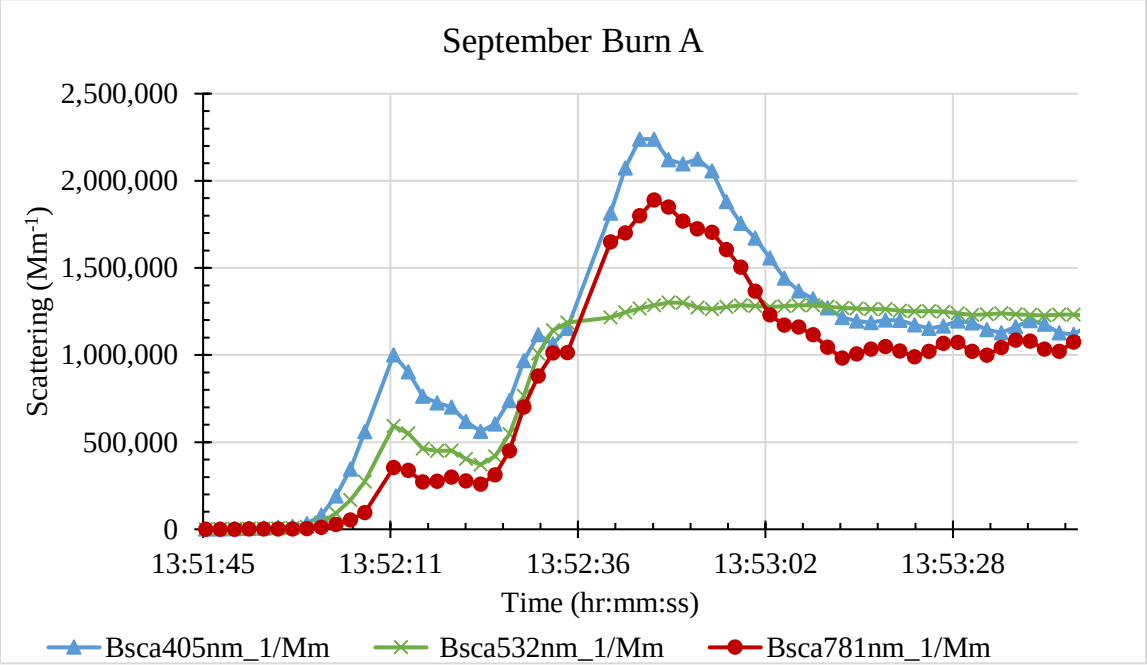

Figure 3: Saturation of the PMT is reached at scattering coefficients above 500,00 Mm^{-1}. This value will be used as a threshold limit for the scattering coefficient.

Next, we will discuss data and results for the Ångström exponents. In figure 4 and figure 5, reasonable values for AAE and SAE are plotted along with the data after the

threshold has been reached. The AAE and SAE values calculated after saturation occurs (i.e., after the threshold limit was exceeded) are marked with a red box. Values of AAE and SAE are reasonable early on in the burn, but after the threshold limit was exceeded, the data were deemed to be unreliable. For the AAE and SAE values of this burn, the results prior to saturation were reasonable. For the SAE, the range of 2.5-3 aligns more with fine mode particles, and the AAE with a range of 2-4.5 indicates there is absorption from BrC.

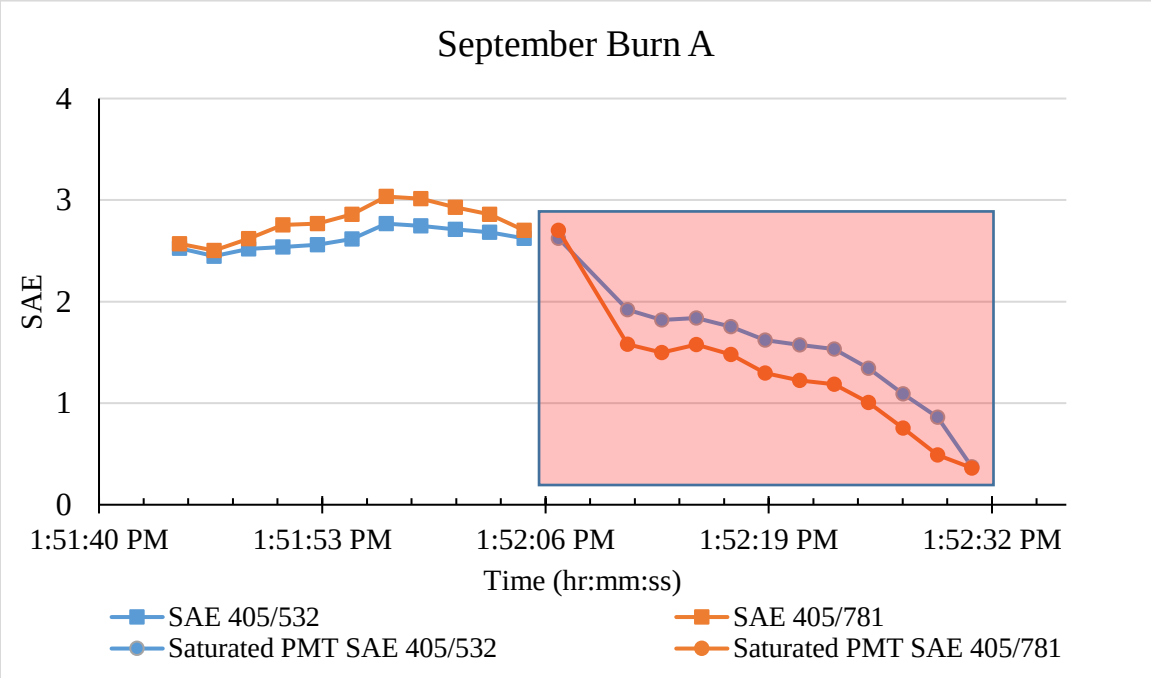

Figure 4: SAE plotted as a function of time including time periods before and after PMT saturation was reached at 1:52:07. Values after the threshold was exceeded are highlighted by the red box.

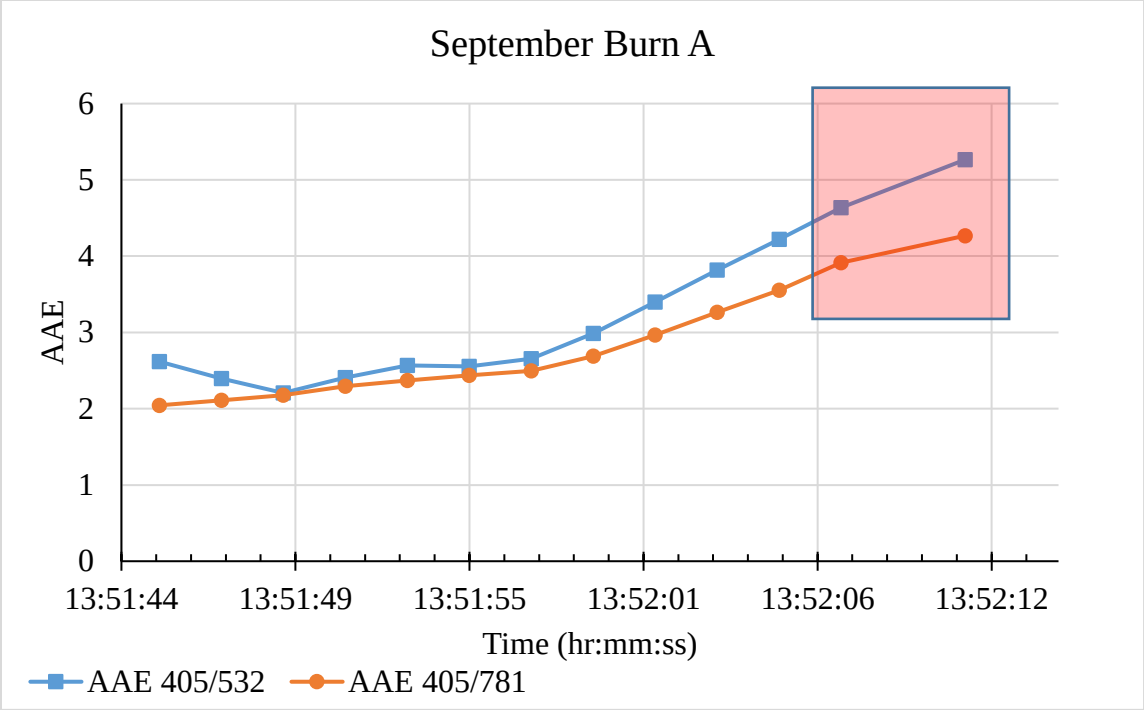

Figure 5: AAE plotted as a function of time. The initial AAE values were in a reasonable range. The transmitted laser power became too low after 1:52:06 and the PMT was overloaded. At 1:52:07 the data becomes unreasonable as the photodetector was impacted and the window became dirty. The points after the threshold has been exceeded are highlighted by the red box.

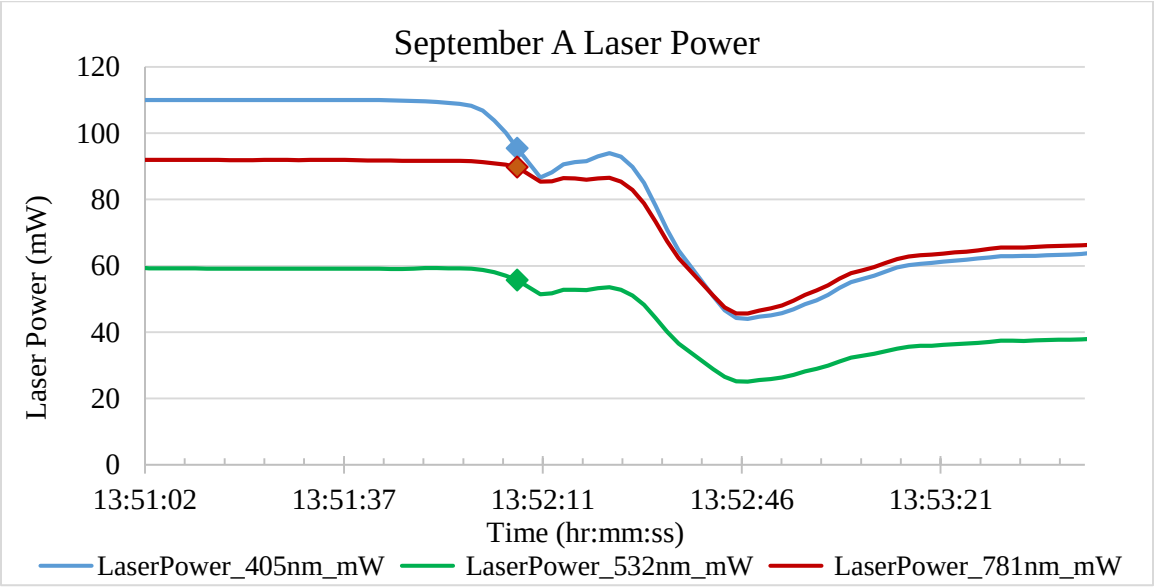

Figure 6: The transmitted laser power was not sustained as excessive particle concentrations in the chamber caused over-saturation of the scattering signal. In addition, the windows became dirtier as smoke particles stuck to their surface, further reducing the measured laser power at the end of the resonator. The markers indicate the time after which the scattering coefficient threshold of 500,000 Mm^{-1} was exceeded.

The transmitted laser power is plotted in figure 6 and it shows a general decrease with time after particle concentrations in the resonator became excessive. The laser power drops, partially recovered when particle concentrations were reduced, but stabilized at a lower power than prior to encountering excessive particle concentrations, likely due to soiled windows. This results in a laser power being measured that is not representative of the power that the particles in the chamber are exposed to and therefore invalidates data.

August Burn C

A burn of August cheatgrass had been performed that did not utilize a sealed chamber. The fan was on and the gate that controls the air flow into the chamber was fully open. The results from this burn were much more reasonable, in line with proper behavior of the PASS-3. The scattering coefficients did not reach the threshold. This method of allowing air to dilute the smoke in the chamber resulted in scattering and absorption coefficients within the measurement range of the PASS-3. Additionally, reduction of the fuel mass burned would also contribute to lower smoke concentration facilitating proper PASS-3 operation.

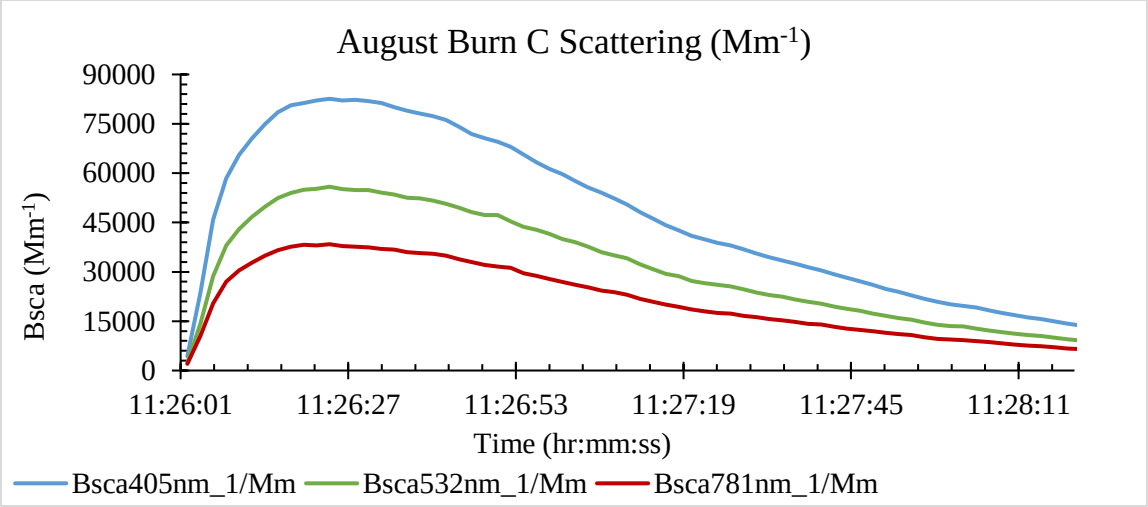

Figure 7: Scattering coefficients for August Burn C that did not reach threshold with the PMT operating without saturation.

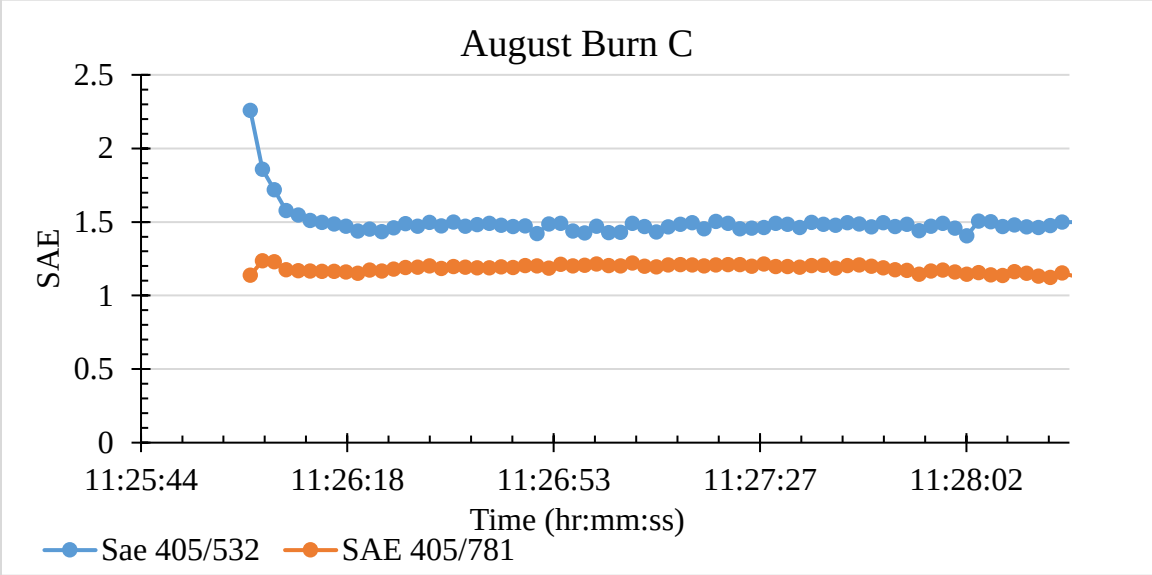

Figure 8: SAE as a function of time. Here, the scattering coefficients (fig. 7) stayed below the threshold value, resulting in more representative SAE values.

In figure 8, the 405/781 nm SAE is more responsive to coarse mode particles while the 405/532 nm SAE is more responsive to fine and medium coarse mode particles. The measured scattering coefficients result in reasonable SAE values. In figure 9, the high values of AAE indicate dominant absorption by BrC with little absorption by BC.

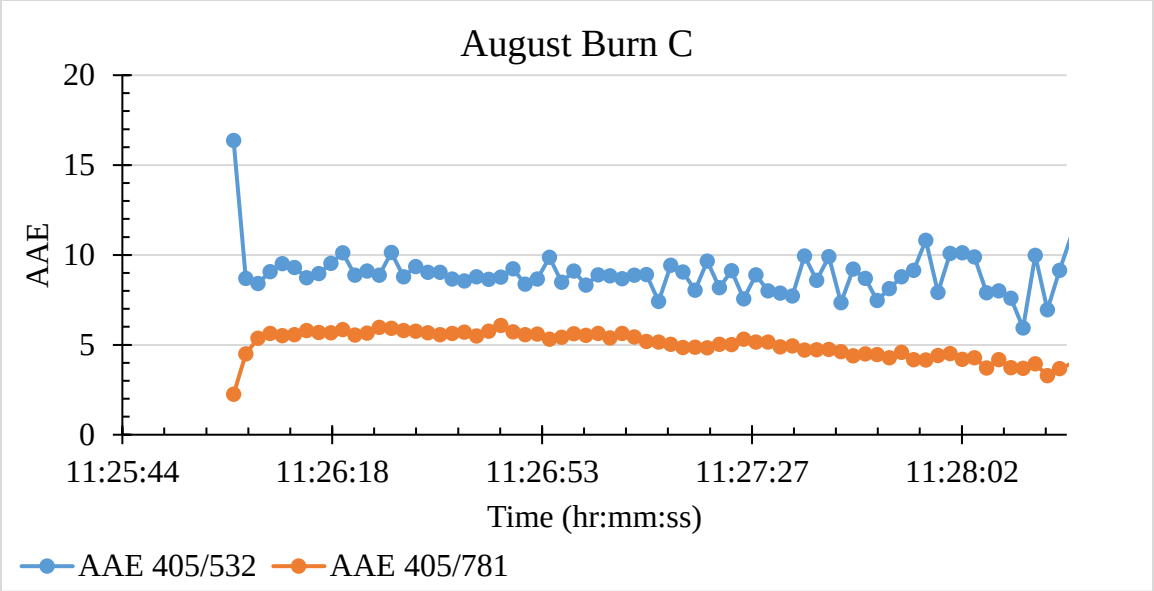

Figure 9: AAE values as a function of time showing reasonable values of AAE.

Absorption and Scattering Ångström Exponents

The AAE is nearly constant (~1) for BC, but is larger than 2 for a mix of BC and BrC (Moosmüller et al. 2011). Here, Ångström exponents were calculated for pairs of 405/532 nm wavelengths and 405/781 nm wavelengths. The differences between 405/532 and 405/781 AAE are most likely driven by BrC absorption that dominates UV absorption and by BC absorption that is less dependent on wavelength. SAE gives information on particle sizes indicating coarse-mode particles for values of <1.5 and fine-mode for SAE values of >1.5 (Hopner et al. 2019). In figure 10, 11, 12, and 13 measured AAE and SAE values are plotted as a function of time for the fuel sample months. Each month, three sample burns were performed and are denoted by A, B, and C.

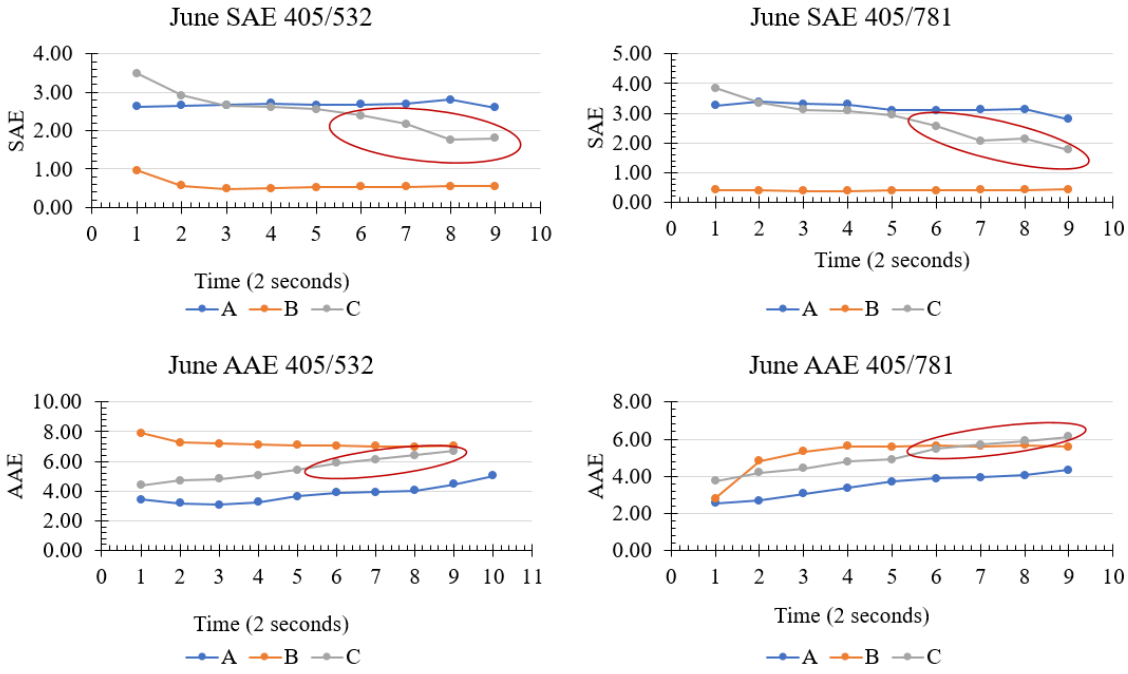

Figure 10: The first values of the June burn experiments SAE and AAE are plotted as a function of time (2 sec.). Data after saturation of the PMT are noted with a red circle. The 3 sample burns were performed denoted by A, B, and C.

The SAE values of June have reasonable values prior to the threshold values being exceeded. The third burn, C, performed reached threshold more rapidly than the previous two burns A and B. Values calculated from saturated data have been noted by red circles. Corresponding 405 nm scattering coefficient are shown in figure 14. The AAE values are also reasonable with enhanced UV absorption from BrC.

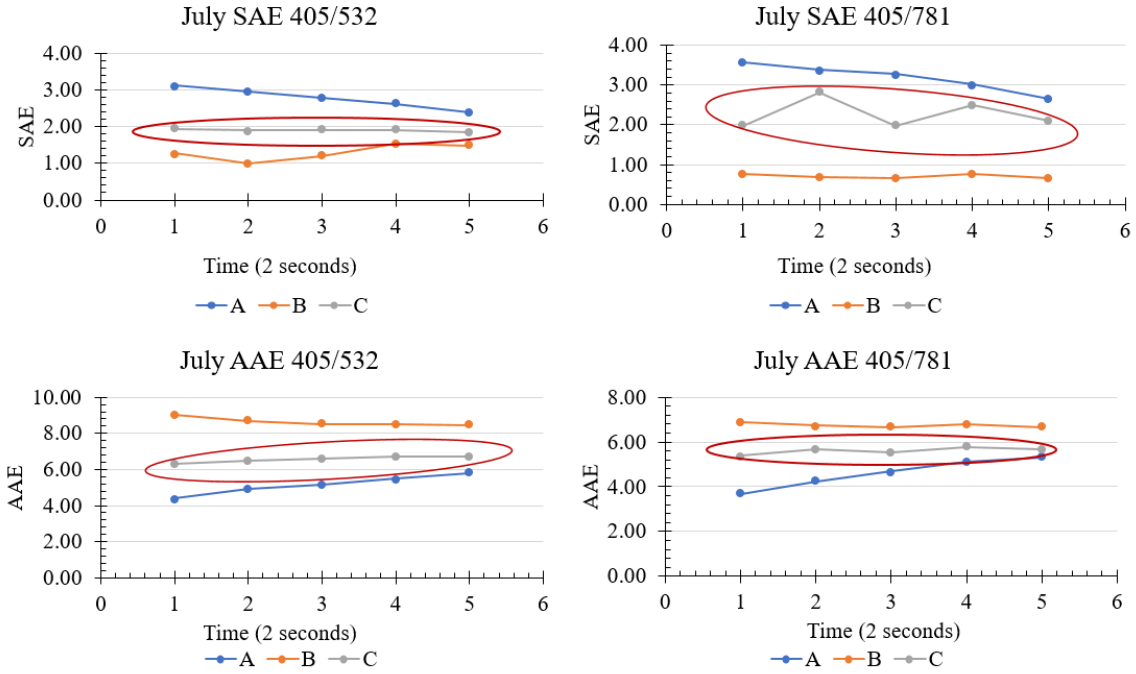

Figure 11: The first values of the July burn experiments SAE and AAE are plotted as a function of time (2 sec.). Data after saturation of the PMT are noted with a red circle. The 3 sample burns were performed denoted by A, B, and C. The x-axis denotes data points recorded every 2 seconds.

The SAE values for July fuels are reasonable prior to the threshold exceeded for burn A and burn C. Burn B reached threshold as soon as sampling started. These saturation points have been noted by the red circle and their corresponding 405 nm scattering coefficient have been plotted in figure 14. The SAE values where threshold has not been exceeded show more scattering due to fine mode particles. The AAE values calculated from valid data indicates higher values of absorption from BrC in the UV wavelengths.

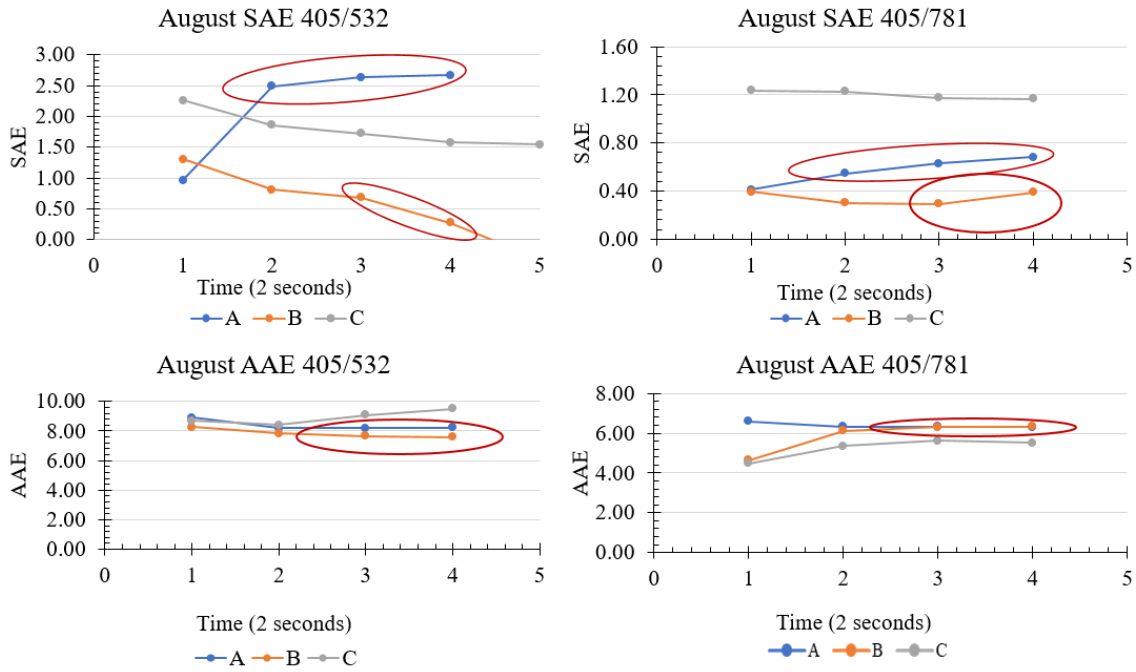

Figure 12: The first values of the August burn experiments SAE and AAE are plotted as a function of time (2 sec.). Data after saturation of the PMT are noted with a red circle.

The SAE values of August have only a few reasonable values prior to the scattering coefficients passing the threshold. Burn B and C reached threshold more rapidly than Burn A though saturation was reached the fastest from the August cheatgrass samples. SAE and AAE values calculated from above threshold data have been marked with red circles and their corresponding 405 nm scattering coefficient have been plotted in figure 14. The AAE values also have few reasonable data points that have been influenced by absorption from BrC in the UV wavelengths.

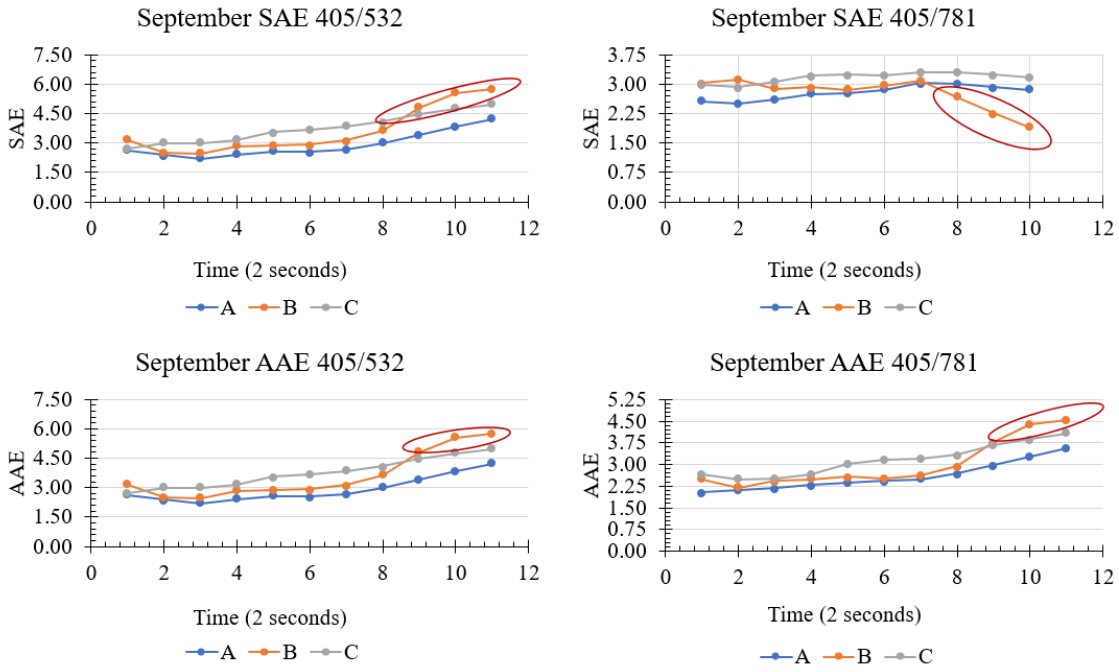

Figure 13: The first values of the September burn experiments SAE and AAE are plotted as a function of time (2 sec.). Data after saturation of the PMT are noted with a red circle.

The SAE values of September have reasonable values prior to the scattering coefficients passing the threshold. Burn C reached threshold more rapidly than Burn A and Burn B. SAE and AAE values calculated from above threshold data have been marked with red circles and their corresponding 405 nm scattering coefficient have been plotted in figure 14. The AAE values also have several reasonable data points before threshold is passed that have been influenced by absorption from BrC in the UV wavelengths.

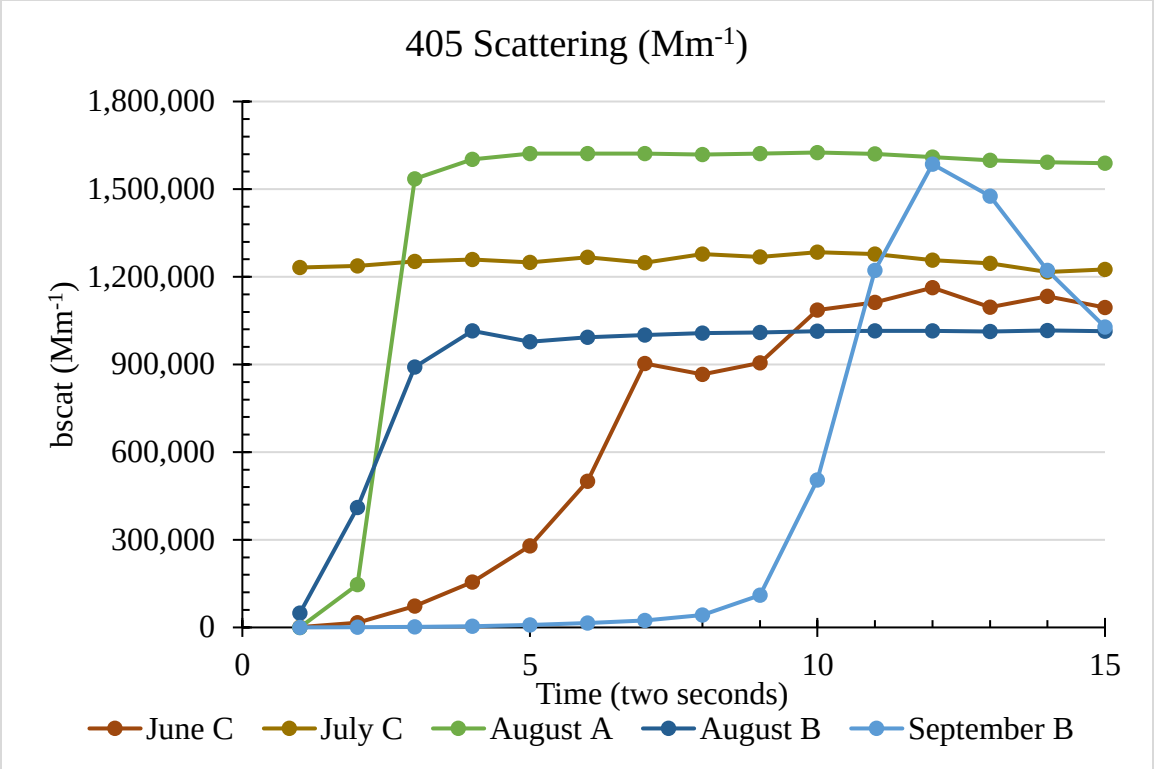

Figure 14: The scattering coefficients (Mm^{-1}) are plotted every two seconds for the measurements where the PMT became saturated after the threshold value of 500,000 Mm^{-1} has been passed.

Emission Factors and comparison to previously reported EFs

The monthly averaged EFs are listed in table 2 along with EFs from a burn experiment performed at DRI in 2014 that have not been published and other values that had previously been reported for similar types of fuel. Table 2 shows that there is little dependence on the month in which cheatgrass fuel was harvested and burned. Cheatgrass EFs determined here compare well with the EFs that had been determined by our lab group in 2014.

In Table 2, we also compare our EFs with previously reported EFs (Urbanski, 2014) for prescribed burns and data from (Chen et al. 2007) who performed open-combustion in

the laboratory similar to the methods used here, and with EFs that were compiled by (Andreae, 2019) in an assessment of EFs from BB in young fire plumes.

	EF_{CO2} (g/kg)	EF_{CO} (g/kg)	EF_{PM} (g/kg)
June	1663.4±25	19.6±24	6.76±1.3
July	1626.3±47	38.4±30	6.54±3.0
August	1569.6±62	74.5±39	7.38±3.0
September	1610.7±19	48.3±12	24.26±6.7
Average	**1617.5±38.8**	**45.2±22.9**	**11.2±8.7**
Cheatgrass 2014	**1493.0±24**	**23.8±1.2**	**32.58±10**
Prescribed Fire Grassland[1]	1705	61	-
Dambo Grass[2]	1606.6±10.2	20.1±4.0	2.2±1.1
Montana Grass[2]	1456.4±15.0	24.8±1.5	10.3±0.9
Savanna and grasslands[3]	1660±90	69±20	8.7±3.1

Table 2: Monthly averages of EFs for cheatgrass are listed with previously reported data from a prescribed burn experiment (Urbanski, 2014)[1] open combustion of Dambo and Montana grass (Chen et al. 2007) [2] and (Andreae, 2019)[3] show good agreement with reported EFs of cheatgrass. Our EFs are listed with the standard error showing the overall variation each month for CO and PM are small but CO_2 sees highly variable emittance.

Our data for both this campaign and the campaign performed in 2014 agree well with the EF_{CO2}, EF_{CO}, and EF_{PM} from the laboratory data presented by Chen et al. (2007), and wildfire plume data reported by Andreae (2019), and S. Urbanski (2014).

Conclusions

Ecosystems in the Great Basin are greatly affected by the invasion of cheatgrass. While cheatgrass has comparatively low available fuel mass for wildland fires compared to the fuel available to burn in conifer or boreal forests, wildland fires will continue to become more frequent and in intense while cheatgrass continues to invade the Great Basin.

The combustion of cheatgrass was observed to be mostly a complete combustion. The smoke contained little BC with high amounts of BrC. Difficulty with optical measurements lead to a threshold being set for the PASS-3. Burn experiments would be

best measured with use of proper dilution and lower fuel mass burned to avoid saturation of photomultiplier tubes. In order to avoid future measurement issues, a preferred method for optical properties would better follow the procedure of the August Burn B allowing air mixing in the chamber. The threshold set in this experiment for the PASS-3 scattering coefficient of 500,000 Mm^{-1} in the 405 nm wavelength is recommended as an upper limit for future burns. Comparison between our monthly fuel burn EF_{CO2}, EF_{CO}, and EF_{PM} , the values calculated in 2014, and other previously reported EFs for grasslands and savannahs show emissions from cheatgrass fires are in numerical agreement with previously reported EFs for other gases and contribute to regional emissions of greenhouse gases during wildland fires.

Acknowledgements:
This project was funded in part by NASA ROSES Grant Number NNX15AI48G and NSF Grant Number AGS-1544425. Thank you for the financial support from the International Association of Wildland Fire (IAWF) MSc Student Scholarship for 2019. Thanks to Environmental Analysis Facility (EAF) of the Desert Research Institute for fuel analysis. We greatly appreciate the assistance from Adam Watts for his advice and knowledge and J. Rennie for assistance with field sample collection.

Reference:

Akagi, S. K., Yokelson, R. J., Wiedinmyer, C., Alvarado, M. J., Reid, J. S., Karl, T., et al. (2011). Emission factors for open and domestic biomass burning for use in atmospheric models. Atmospheric Chemistry and Physics, 11(9), 4039-4072.

Andreae, M. O. (2019). Emission of trace gases and aerosols from biomass burning - an updated assessment. Atmospheric Chemistry and Physics, 19 (13), 8523-8546.

Arnott, W. P., Moosmüller, H., Rogers, C. F., Jin, T. F., & Bruch, R. (1999). Photoacoustic spectrometer for measuring light absorption by aerosol: instrument description. Atmospheric Environment, 33 (17), 2845-2852.

Beck, G. (2012). Cheatgrass and Wildfire. In C. S. University (Ed.), Natural Resources Series, Fact Sheet No. 6.310 (pp. 3). Colorado State University: Colorado State Forest Service, Colorado State University, Fort Collins, CO.

Bradley, B. A., Curtis, C. A., Fusco, E. J., Abatzoglou, J. T., Balch, J. K., Dadashi, S., et al. (2018). Cheatgrass (*Bromus tectorum*) distribution in the intermountain Western United States and its relationship to fire frequency, seasonality, and ignitions. Biological Invasions, 20 (6), 1493-1506.

Bradley, B. A., Houghtonw, R. A., Mustard, J. F., & Hamburg, S. P. (2006). Invasive grass reduces aboveground carbon stocks in shrublands of the Western US. Global Change Biology, 12 (10), 1815-1822.

Chen, L. W. A., Moosmüller, H., Arnott, W. P., Chow, J. C., Watson, J. G., Susott, R. A., et al. (2007). Emissions from laboratory combustion of wildland fuels: Emission factors and source profiles. Environmental Science & Technology, 41 (12), 4317-4325.

Chylek, P., & Wong, J. (1995). Effect of absorbing aerosols on global radiation budget. Geophysical Research Letters, 22 (8), 929-931.

Dantonio, C. M., & Vitousek, P. M. (1992). Biological Invasions by Exotic Grasses, the Grass Fire Cycle, and Global Change. Annual Review of Ecology and Systematics, 23, 63-87.

Davies, K. W., & Nafus, A. M. (2013). Exotic annual grass invasion alters fuel amounts, continuity and moisture content. International Journal of Wildland Fire, 22 (3), 353-358.

Hassan, T., Moosmuller, H., & Chung, C. E. (2015). Coefficients of an analytical aerosol forcing equation determined with a Monte-Carlo radiation model. Journal of Quantitative Spectroscopy & Radiative Transfer, 164, 129-136.

Hopner, F., Bender, F. A. M., Ekman, A. M. L., Andersson, A., Gustafsson, O., & Leck, C. (2019). Investigation of Two Optical Methods for Aerosol-Type Classification Extended to a Northern Indian Ocean Site. Journal of Geophysical Research-Atmospheres, 124 (15), 8743-8763.

Martinsson, J., Eriksson, A. C., Nielsen, I. E., Malmborg, V. B., Ahlberg, E., Andersen, C., et al. (2015). Impacts of Combustion Conditions and Photochemical Processing on the Light Absorption of Biomass Combustion Aerosol. Environmental Science & Technology, 49 (24), 14663-14671.

McMeeking, G. R., Kreidenweis, S. M., Baker, S., Carrico, C. M., Chow, J. C., Collett, J. L., et al. (2009). Emissions of trace gases and aerosols during the open combustion of biomass in the laboratory. Journal of Geophysical Research-Atmospheres, 114, 20.

McMeeking, G. R., Kreidenweis, S. M., Baker, S., Carrico, C. M., Chow, J. C., Collett, J. L., et al. (2009). Emissions of trace gases and aerosols during the open combustion

of biomass in the laboratory. Journal of Geophysical Research-Atmospheres, 114, 20.

Moosmüller, H., & Chakrabarty, R. K. (2011). Technical Note: Simple analytical relationships between Angstrom coefficients of aerosol extinction, scattering, absorption, and single scattering albedo. Atmospheric Chemistry and Physics, 11 (20), 10677-10680.

Moosmüller , H., Chakrabarty, R. K., & Arnott, W. P. (2009). Aerosol light absorption and its measurement: A review. Journal of Quantitative Spectroscopy & Radiative Transfer, 110 (11), 844-878.

Moosmüller, H., Chakrabarty, R. K., Ehlers, K. M., & Arnott, W. P. (2011). Absorption Angstrom coefficient, brown carbon, and aerosols: basic concepts, bulk matter, and spherical particles. Atmospheric Chemistry and Physics, 11 (3), 1217-1225.

Moosmüller , H., Engelbrecht, J. P., Skiba, M., Frey, G., Chakrabarty, R. K., & Arnott, W. P. (2012). Single scattering albedo of fine mineral dust aerosols controlled by iron concentration. Journal of Geophysical Research-Atmospheres, 117, 10.

Moosmüller, H., & Sorensen, C. M. (2018a). Single scattering albedo of homogeneous, spherical particles in the transition regime. Journal of Quantitative Spectroscopy & Radiative Transfer, 219, 333-338.

Moosmüller, H., & Sorensen, C. M. (2018b). Small and large particle limits of single scattering albedo for homogeneous, spherical particles. Journal of Quantitative Spectroscopy & Radiative Transfer, 204, 250-255.

Pistone, K., Redemann, J., Doherty, S., Zuidema, P., Burton, S., Cairns, B., et al. (2019). Intercomparison of biomass burning aerosol optical properties from in situ and remote-sensing instruments in ORACLES-2016. Atmospheric Chemistry and Physics, 19 (14), 9181-9208.

Rein, G. u. (2016). Smoldering Combustion. In H. M. J. e. al. (Ed.), SFPE Handbook of Fire Protection Engineering (pp. pp 581-603). New York, NY: Springer, New York, NY.

Samburova, V., Connolly, J., Gyawali, M., Yatavelli, R. L. N., Watts, A. C., Chakrabarty, R. K., et al. (2016). Polycyclic aromatic hydrocarbons in biomass-burning emissions and their contribution to light absorption and aerosol toxicity. Science of the Total Environment, 568, 391-401.

Satheesh, S. K., & Moorthy, K. K. (2005). Radiative effects of natural aerosols: A review. Atmospheric Environment, 39 (11), 2089-2110.

Selimovic, V., Yokelson, R. J., Warneke, C., Roberts, J. M., de Gouw, J., Reardon, J., et al. (2018). Aerosol optical properties and trace gas emissions by PAX and OP-FTIR for laboratory-simulated western US wildfires during FIREX. Atmospheric Chemistry and Physics, 18 (4), 2929-2948.

Stocks, B. J., Fosberg, M. A., Lynham, T. J., Mearns, L., Wotton, B. M., Yang, Q., et al. (1998). Climate change and forest fire potential in Russian and Canadian boreal forests. Climatic Change, 38 (1), 1-13.

Tian, J., Chow, J. C., Cao, J. J., Han, Y., Ni, H. Y., Chen, L. W. A., et al. (2015). A Biomass Combustion Chamber: Design, Evaluation, and a Case Study of Wheat Straw Combustion Emission Tests. Aerosol and Air Quality Research, 15 (5), 2104-2114.

Urbanski, S. (2014). Wildland fire emissions, carbon, and climate: Emission factors. Forest Ecology and Management, 317, 51-60.

Urbanski, S. P. (2013). Combustion efficiency and emission factors for wildfire-season fires in mixed conifer forests of the northern Rocky Mountains, US. Atmospheric Chemistry and Physics, 13 (14), 7241-7262.

Urbanski, S. P., Reeves, M. C., Corley, R. E., Silverstein, R. P., & Hao, W. M. (2018). Contiguous United States wildland fire emission estimates during 2003-2015. Earth System Science Data, 10 (4), 2241-2274.

Chapter 2

Gaseous Elemental Mercury Emissions from the Open Laboratory Combustion of Cheatgrass (*Bromus Tectorum*)

M. Rennie[1,2], D. Obrist[3], H. Moosmüller[1]
[1]Division of Atmospheric Sciences, Desert Research Institute, Reno, NV, USA
[2] University of Nevada-Reno, Reno, NV, USA
[3]Department of Environmental, Earth & Atmospheric Sciences at University of Massachusetts Lowell

Abstract

Cheatgrass (*Bromus Tectorum*), an invasive species dominant in the Great Basin of the Western U.S., grows in early spring and dries by early summer supplying large amounts of highly flammable fuel to sagebrush and other ecosystems. This facilitates an earlier, more active fire season that is changing the landscape ecology in the Great Basin. Despite, the importance of cheatgrass for the fire ecology of large parts of the western U.S., emission factors for its combustion are largely unknown. Here, we quantify gaseous elemental mercury (GEM) emission factors from the laboratory combustion of cheatgrass and showed that they are comparable to those of South African savanna grasses.

Introduction

Mercury (Hg), a toxic heavy metal, is ubiquitous in the environment in its elemental form and in organic and inorganic materials (Schroeder & Munthe, 1998). Mercury is emitted into the atmosphere through anthropogenic processes such as mining or combustion of fossil and biofuels and through natural processes including volcanos and biomass burning (BB). In the atmosphere, mercury is primarily found as gaseous elemental mercury (GEM) which is relatively inert and rarely affected by oxidation (Friedli et al. 2003). In addition to GEM (Hg°), two other oxidation states, reactive (Hg^{2+}), and particle

bound (Hg^P), are found in the atmosphere. However, GEM accounts for 95% of atmospheric mercury mass loading (Millhollen, Gustin, & Obrist 2006; Obrist et al. 2008) and is a global pollutant with an atmospheric lifetime of ~1 year (Wiedinmyer & Friedli 2007); its eventual deposition is controlled by meteorological and surface parameters (Lyman et al. 2007).

BB is considered to be a significant source of mercury emissions into the atmosphere (Finley, Swartzendruber, & Jaffe 2009; Obrist et al. 2008), and global wildfire activity and resulting BB mercury emissions have increased due to climate change and anthropogenic activities (Seo et al. 2016). Mercury in biomass fuels originates mostly from atmospheric mercury (Ericksen et al. 2003) through dry and wet deposition being taken up by foliage (Niu et al. 2011; Rea et al. 2002), mostly through the stomata (Huang et al. 2011; Rutter et al. 2011). Plants have been discovered to be a sink of GEM (Ericksen et al. 2003). During BB events, like prescribed burns and wildfires, mercury contained in biomass fuels is re-emitted into the atmosphere, mostly as gaseous elemental mercury (GEM), as part of the global mercury cycle (Wiedinmyer & Friedli 2007).

North America's largest desert, the Great Basin, spans most of Nevada, much of Utah, and smaller parts of Oregon, California, Idaho and Wyoming. The native ecology is dominated by a mix of sagebrush (*Artemisia Tridentata*), shrubs and undergrowth of forbs and native grasses. Wildfire activity in the Great Basin has increased in size and frequency due to the increased occurrence of noxious weeds and exotic annual grasses (Bradley et al. 2018), implying a corresponding increase in mercury emissions.

Cheatgrass (*Bromus Tectorum*) is an invasive grass that has extensive ecological impacts in the Great Basin (Bradley et al. 2018) with the ability to produce over 10,000 plants in a square mile (Beck 2012). Cheatgrass is increasing the frequency and extent of rangeland fires ten-fold (Bradley et al. 2006) by creating higher fuel loads with low fuel moisture early in summer. Areas invaded by cheatgrass experience higher spatial vegetative coverage in areas where shrubs and desert grasses were once separated by mostly open areas of soil. Areas where the cheatgrass coverage has grown to ≥ 15% are more than twice as likely to burn compared to areas where the cheatgrass coverage is low (Bradley et al. 2018). Cheatgrass coverage is rapidly growing throughout the Great Basin. The purpose of this study is to present a first assessment of fuel-based GEM emission factors for open cheatgrass combustion and compare them with those of other grasses.

Methods

This study was conducted with cheatgrass fuel collected over the spring and summer of 2019 from a sample site 39°28’58” N and 119°51’57” W at the western edge of Reno, NV, USA at site of the Hawken fire of June 2016. This fire burned through sagebrush and chaparral, consequently increasing the amount of cheatgrass, within its perimeter. Reno, NV is located at the western edge of the Great Basin with lower elevations typically covered in sagebrush steppe where cheatgrass is most invasive and persistent. Starting in June and continuing through September 2019, cheatgrass samples were collected monthly from this site. Vegetation samples were collected using new latex gloves and Zip-lock bags to reduce fuel contamination.

The biomass burning experiment took place in the burn chamber at the Desert Research Institute (DRI) biomass burning facility, a close replicate of this facility has previously been described in Tian et al. (2015). The facility consists of sealable chamber with aluminum walls (1.8 m x 1.8 m x 2.06 m) that taper at the roof in a pyramid (1.8 m x 1.8m x 0.6 m). This allows smoke to be funneled into an exhaust pipe where multiple sampling ports are attached, and copper pipe sampling tubes are used to deliver BB emissions to multiple instruments for real-time measurements. The flow through the chamber can be controlled with an adjustable inlet gate located beneath the fuel bed in conjunction with a controllable fan that exhausts air out of the chamber. As our cheatgrass samples (~100 g) burned rapidly, with quickly changing emissions, we closed off the chamber, by turning off the fan and fully closing the gate, to accumulate emissions for characterization of emissions averaged over individual burns, similar to the methods used by McMeeking et al. (2009).

Analysis instruments included (1) a CO Thermo 48i carbon monoxide analyzer, (2) a CO_2 analyzer (Li-7000 CO_2/H_2O Analyzer, Lincoln, NE, USA), that each sampled every second with a 1 l/min flow rate, and (3) a Tekran mercury analyzer (Tekran 2537A, Toronto, ON, Canada) connected to the sampling tube with 1/8" OD Teflon tubing. The cheatgrass fuel was arranged on top of the ceramic fuel bed and the loss of fuel mass was monitored in real time using a Veritas L Series Precision balance (0.01 g of precision) throughout the burn.

A Tekran 2537A mercury analyzer was used to quantify the amount of GEM in the smoke with a sampling time of 2.5-minute at a flow rate of 1.5 l/min. A 1-μm pore diameter

PTFE filter was inserted into the middle of the sampling line and another 0.2-um pore diameter Teflon filter was placed in the Tekran inlet to eliminate particulate matter from the sample. During the collection cycle, GEM is collected onto gold traps, followed by desorption and analysis with cold vapor atomic fluorescence spectrometry (Fitzgerald & Gill, 1979). Calibration of the Tekran was preformed using the internal permeation source. Total mercury contents in the fuels and ash were evaluated with a direct mercury analyzer (Milestone Inc., Model DMA-80, Sorisole, BG, Italy) at the Department of Environmental, Earth & Atmospheric Sciences (EEAS) of the University of Massachusetts, Lowell, MA, USA.

The monthly samples of cheatgrass were burned in triplicate and results were averaged. Cheatgrass was piled on top of the ceramic disk in the chamber to monitor fuel mass loss during the burning period. The copper pipe that connected the chamber to the real-time sampling instruments was disconnected and the fuel was ignited with a lighter. The chamber was allowed to fill with smoke for 5 minutes to integrate emissions over the burn. The 5-minute period allowed the Tekran to begin sampling at the beginning of a new cycle. Within ten seconds of the 5-minute time period, the copper pipes and the Teflon tubing for the Tekran were reconnected to the chamber. The real-time instruments then characterized smoke from the chamber until concentrations decayed to near ambient conditions. The peak of the GEM mass concentrations as function of time are plotted for 12 burns in figure 1, illustrating accumulation of GEM during the burn and its subsequent decay to near-ambient concentrations.

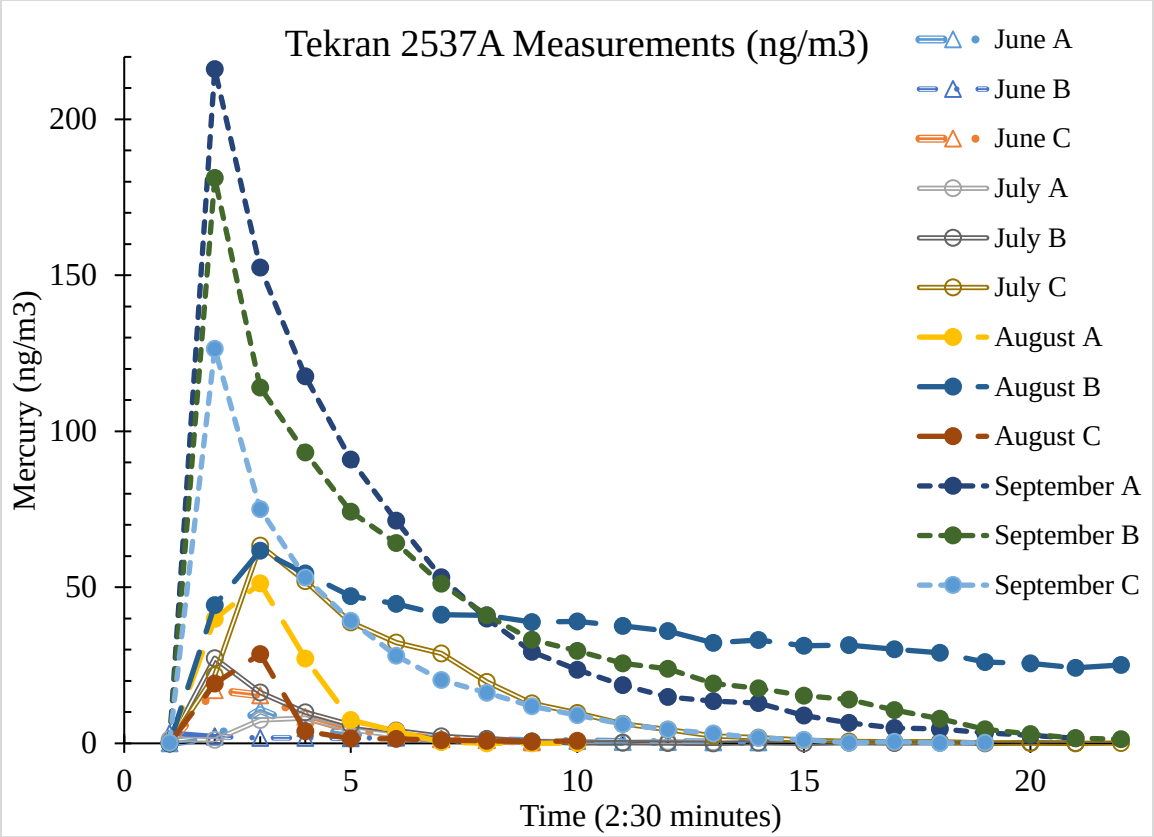

Figure 1: Peak values of the measurements of GEM that were measured by the Tekran 2537A (2:30 minute intervals) shown above illustrate the differences in the emitted mercury between burns.

Emission Factors

Fuel-based GEM emission factors (EF_{GEM}) can be calculated as the ratio of GEM mass emitted (M_{GEM}) to dry fuel mass combusted (M_{fuel}) as

$$EF_{GEM} = \frac{M_{GEM}}{M_{fuel}} \quad (1a)$$

In order to account for the air dilution in the chamber, we multiply by the chamber volume of $V_{chamber}$

$$EF_{GEM} = \frac{M_{GEM}}{M_{fuel}} * V_{chamber} \quad (1b)$$

The maximum mass concentration of GEM in the chamber and the fuel mass consumed during each burn is reported in Table 1. The GEM peak concentration gives a good approximation of the GEM emitted during the burn.

	C_{GEM} (ng/m^3)	**Fuel Combusted (g)**	**C_{GEM}*V (ng)**	**EF_{GEM} (ng/g)**
June (Burn A)	10.6±0.07	41.5±0.01	82.4±0.05	2.0±0.06
June (Burn B)	17.1±0.06	68.1±0.01	132.9±0.05	2.0±0.06
June (Burn C)	28.3±0.09	63.3±0.01	220.2±0.05	3.5±0.06
July (Burn A)	8.1±0.02	82.0±0.01	63.0±0.05	0.8±0.06
July (Burn B)	27.4±0.06	56.8±0.01	213.0±0.05	3.8±0.06
July (Burn C)	63.4±0.01	77.7±0.01	493.9±0.05	6.4±0.06
August (Burn A)	51.6±0.04	86.2±0.01	401.8±0.05	4.7±0.06
August (Burn B)	28.6±0.10	79.8±0.01	223.1±0.05	2.8±0.06
August (Burn C)	61.8±0.09	79.6±0.01	481.4±0.05	6.1±0.06
September (Burn A)	217.7±0.08	86.1±0.01	1695.5±0.05	19.7±0.06
September (Burn B)	181.2±0.10	83.6±0.01	1411.6±0.05	16.9±0.06
September (Burn C)	126.5±0.04	88.5±0.01	985.1±0.05	11.1±0.06

Table 1: Mercury emission factors are calculated using measured GEM multiplied by the chamber volume over the fuel mass combusted. The variability between each of the monthly fuel burns are due to the changes in fuel composition (more or less seeds, stems, or leaves) and the erratic behavior of biomass fuel combustion.

Next EFs were calculated with a different method using the ratio of GEM mass concentration to carbon mass emitted (EF_{Hg}) as

$$EF_{GEM} = \frac{M_{GEM}}{M_{fuel}} \tag{2a}$$

where (M_{GEM}) is the ratio of mercury mass concentration emitted to dry fuel mass combusted (M_{fuel}). M_{fuel} was determined as the ratio of total carbon mass emitted (M_C) and the carbon mass fraction of the dry fuel (CMF_{fuel}) as

$$M_{fuel} = \frac{M_C}{CMF_{fuel}}, \tag{2b}$$

where the total carbon mass emitted (M_C) is well approximated by the sum of carbon mass in carbon dioxide ($M_{C_{CO_2}}$) and carbon monoxide ($M_{C_{CO}}$) as

$$M_C = M_{C_{CO_2}} + M_{C_{CO}} = \frac{12}{44} M_{C_{CO_2}} + \frac{12}{28} M_{CO}, \quad (2c)$$

This gives an equation for (EF_{GEM}) as the total ratio of carbon mass emitted as

$$EF_{GEM} = \frac{M_{GEM}}{M_{fuel}} = \frac{M_{GEM}}{M_C} * CMF_{fuel} = \frac{C_{GEM}}{C_C} * CMF_{fuel} = \frac{C_{GEM}}{\frac{12}{44} C_{CO_2} + \frac{12}{28} C_{CO}} * CMF_{fuel}, \quad (2d)$$

In this equation we ignore the ash carbon content which is typically less than 5% of the fuel mass Chen et al. (2007). The CMF_{fuel} was determined as part of fuel analyzed with a Thermo Scientific™ EA 1112 Series CHNS-O Analyzer (Waltham, MA, USA) for total carbon, nitrogen, hydrogen, and oxygen percent mass of the sample, with results listed in table 2, at the DRI's Environmental Analysis Facility (EAF).

%Nitrogen	%Carbon	%Hydrogen	%Oxygen	Total%
0.07	46.12	6.31	46.08	98.57

Table 2: Fuel samples were analyzed in triplicate and averaged over all cheatgrass samples. These values are the average ratios determined with the CHNS-O.

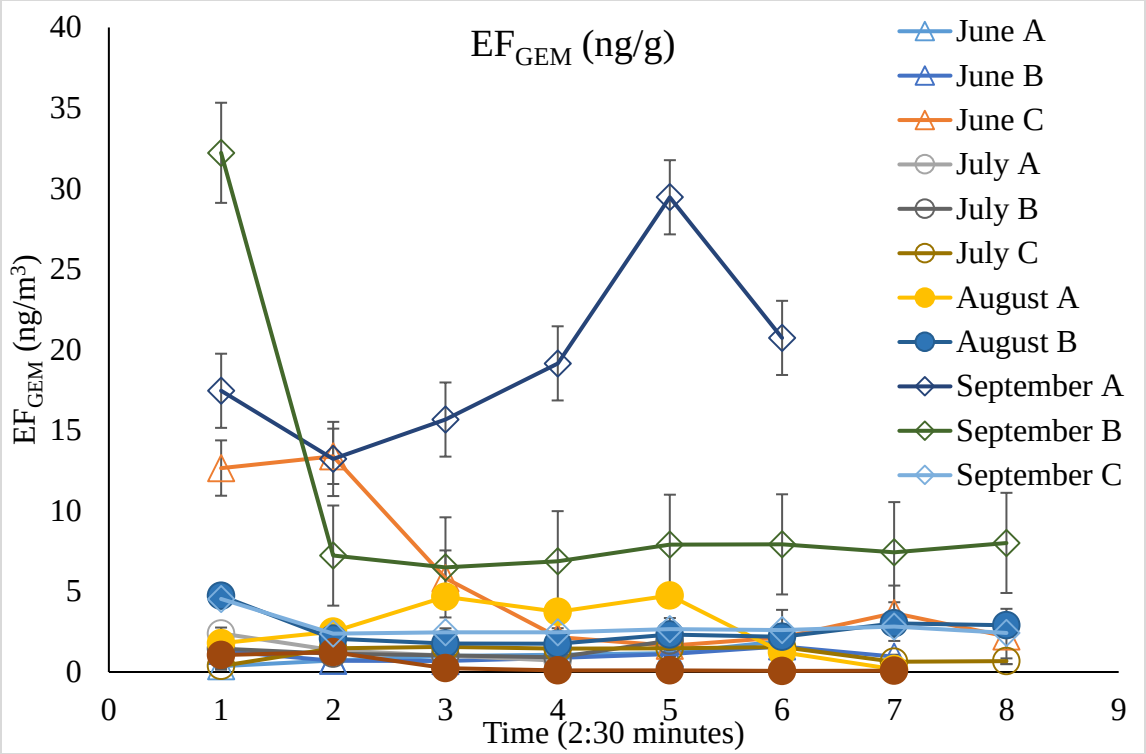

Figure 2: EF (ng/g) of fuel based carbon emissions are plotted with the standard error. September A and B had the largest values of EFs. This data is calculated from the use of the carbon emitted by the CO_2 and CO which is then multiplied by the carbon mass fraction of the fuel.

The plot in figure 2 illustrates the temporal changes of the carbon mass EF_{GEM} that were measured in the chamber. The results show that EFs for June, July, and August remained within the range of 1.4-4.8 while September emitted much higher amounts of GEM.

Emission Factors	**Fuel Consumed (ng/g)**	**Total C mass (ng/g)**
June	2.47±0.87	4.77±3.95
July	3.63±2.0	1.40±0.58
August	4.5±1.6	2.52±1.12
September	15.9±4.4	18.07±8.0

Table 3: Fuel based emission factors were measured in triplicate and averaged. The first column is the monthly average value from equation (1b). The second column is the monthly average values from equation (2d). The errors note the standard error.

Data in table 3 show values for both fuel mass burned EFs and carbon mass emitted EFs calculation methods. The values for the fuel-based emission factors are a single value that is averaged over the monthly burns (i.e. three burns). Cheatgrass fuel burned rapidly and fuel mass loss was completed within 1-2 minutes after ignition before the chamber was connected to sampling instrumentation. Therefore, there is only a single value reported for the fuel based EFs. There are significant differences (i.e. > 21%) between the monthly burns. There is also a significant difference between the methods of calculation. Here, the fuel-mass consumed is the preferred method of calculation for the EFs due to the lower standard errors.

Comparison to other studies

Since GEM emission factors from cheatgrass burns have previously not been reported, we are presenting a comparison with previously determined EF for similar fuels including emissions from grassland and savanna fires listed in Table 4. Friedli et al. (2009) modeled biomass burning emissions using estimated burn areas and biomass density/fuel. Cinnirella & Pirrone (2006) used ground surveys of burnt areas of country-based emissions and a combination of remote sensing and the Geographic Information System (GIS) to improve Hg emission estimates for forest fires. Engle et al. (2006) lyophilized samples from a desert wildfire site to find total Hg mass concentration through thermal decomposition, amalgamation, and atomic absorption spectrometry for soil samples of a Nevada sagebrush steppe. Streets et al. (2005) modeled anthropogenic Hg emissions in China from statistical data. Chen et al. (2013) and Zhou et al. (2017) compiled EF from all over China. Our EFs quantitatively agree with the South African savanna and the

September EFs are similar to the lower range of the Nevada sage EFs found in the literature. The cheatgrass growing season is much shorter (i.e. s few weeks) compared with grasslands that can grow for a few months. Mercury accumulation will be lower in cheatgrass because it has a much smaller growing period when it would be able to absorb mercury through its stomata.

Emission Factors Fuel Type	**(ng/g)**		**Reference**
June Cheatgrass	2.47±0.50	L	This study
July Cheatgrass	3.63±1.61	L	This study
August Cheatgrass	4.50±0.94	L	This study
September Cheatgrass	15.9±2.53	L	This study
South African savanna	3.0-9.0	L	Friedli et al. 2008
Oregon wheat	38	S	Friedli et al. 2003
Nevada sage	18.7 - 39.9	S	Engle et al. 2006*
Grassland fire	80±41.8	P	Streets et al. 2005°
Mediterranean, Wildfire	51.11	P	Cinnirella & Pirrone 2006
Grass Stems	24	P	Huang et al. 2011
Grass Leaves	34	P	Huang et al. 2011,
Open Shrublands	80	P	Streets et al. 2005, Friedli et al. 2003^

Table 4: EF values from the monthly laboratory burns of cheatgrass are compared with previously published literature data on grassland and sagebrush EFs. L is for laboratory burns, P is for plume measurements taken during wildland burning emissions, and S is for soil. *Range values reported by Wiedinmyer & Friedli (2007), ° values reported by Chen et al. (2013), ^ values reported by Zhou et al. (2017)

Combustion Completeness

Cheatgrass samples and post burn-ash samples for the months of June, July, and August were sent to EEAS at UMass, Lowell. The samples were ground to a fine powder in a stainless-steel coffee mill. Total Hg mass concentrations of the samples were measured using cold-vapor atomic adsorption with preconcentration of samples on gold traps with a Milestone Inc., Model DMA-80 in accordance with U.S. EPA Method 7473. The calibration was based on standard solutions (100 μg L^{-1} and 10 μg L^{-1}) that were formulated

according to EPA Method 1631. Solid standard reference materials (# 1515: Apple Leaves: 44.4 µg Hg kg^{-1}) from the National Institute of Standards and Technology (NIST) were measured prior to and at the end of each sample analysis run. Table 5 lists the month of cheatgrass samples and ash samples that were analyzed. All samples were measured in triplicate and averaged.

Cheatgrass	**concentration (ng/g)**	**std. dev (n=3)**
June	4.80	1.44
July	6.27	0.59
August	7.35	0.46
Ash	**concentration (ng/g)**	**std. dev (n=3)**
June	1.18	0.02
July	0.63	0.11
August	1.21	0.33

Table 5: Cheatgrass samples and the post-burn ash were analyzed for the total mass concentration of Hg.

Previous studies including (Huang et al. 2011) have found that fuel mercury is typically completely released into the atmosphere during burns yet for our cheatgrass fuel samples this was not the case. For June samples, ~27%, ~16%, and ~20% for June, July, and August fuel samples, respectively. This may be due to the rapid combustion of cheatgrass, compared to other fuels, that may not completely release fuel mercury, but result in ~20% of the fuel mercury remaining in the ash.

Conclusion

Wildland fires are growing and changing the ecology of the USIMW into cheatgrass dominated monocultures. Biomass burning is a significant source of gaseous elemental mercury in the atmosphere which is readily taken up by plants (Lyman et al. 2007). As climate change is increasing the frequency and intensity of wildfires, it is

creating future uncertainties in wildland fire emissions. While there has been little previous laboratory work characterizing biomass-burning emissions of GEM (Obrist et al. 2008), there are many calculations of GEM emissions in wildfire plumes and from fire-affected soils.

The emission factors reported in our study are compared to emission factors for savanna, wheat, grasslands, and sagebrush fires which have been determined using various methods. Some of the variation between our EFs and reported EFs for similar fuels may result in from differences in laboratory emissions and wildfire emissions due to increased emission of GEM from fire-affected soils (Friedli et al. 2003) that would not be captured by laboratory combustion. These values can also be variable across regions where atmospheric mercury concentrations are affected by dry/wet deposition rates and locality to cities where larger mercury pools may be available due to anthropogenic emissions. Cheatgrass emission factors are in quantitative agreement with the values for South African savanna previously published literature. Cheatgrass emission factors are mostly lower than those in previously published literature for EFs from wildland fire plumes by a factor of ten.

In this work we present the emission factors of cheatgrass over the growing period in early spring through summer as the plants dried out. Though they are small compared to the emission factors from prescribed grassland fire burns and laboratory burns of other grasses, cheatgrass holds the ability to consistently contribute mercury to the atmosphere. This is due to areas where spatial cheatgrass coverage reaches more than 15% (Bradley et al., 2018) becoming more than twice as likely to experience a wildfire. The emission factors

for cheatgrass combustion will play an increasingly important role in quantifying annual emission, as cheatgrass further invades sagebrush steppes and the open desert. It will be beneficial to take cheatgrass GEM emission factors into consideration when evaluating emissions and transport of gaseous elemental mercury emissions from biomass burning.

Acknowledgements:
This project was funded in part by NASA ROSES Grant Number NNX15AI48G and NSF Grant Number AGS-1544425. We greatly appreciate the assistance from Adam Watts for his advice and knowledge and J. Rennie for assistance with field sample collection.

References

Akagi, S. K., Yokelson, R. J., Wiedinmyer, C., Alvarado, M. J., Reid, J. S., Karl, T., et al. (2011). Emission factors for open and domestic biomass burning for use in atmospheric models. Atmospheric Chemistry and Physics, 11(9), 4039-4072.

Andreae, M. O. (2019). Emission of trace gases and aerosols from biomass burning - an updated assessment. Atmospheric Chemistry and Physics, 19(13), 8523-8546.

Beck, G. (2012). Cheatgrass and Wildfire. In C. S. University (Ed.), Natural Resources Series, Fact Sheet No. 6.310 (pp. 3). Colorado State University: Colorado State Forest Service, Colorado State University, Fort Collins, CO.

Bradley, B. A., Curtis, C. A., Fusco, E. J., Abatzoglou, J. T., Balch, J. K., Dadashi, S., et al. (2018). Cheatgrass (*Bromus tectorum*) distribution in the intermountain Western United States and its relationship to fire frequency, seasonality, and ignitions. Biological Invasions, 20(6), 1493-1506.

Bradley, B. A., Houghtonw, R. A., Mustard, J. F., & Hamburg, S. P. (2006). Invasive grass reduces aboveground carbon stocks in shrublands of the Western US. Global Change Biology, 12(10), 1815-1822.

Chen, C., Wang, H. H., Zhang, W., Hu, D., Chen, L., & Wang, X. J. (2013). High-resolution inventory of mercury emissions from biomass burning in China for 2000-2010 and a projection for 2020. Journal of Geophysical Research-Atmospheres, 118(21), 12248-12256.

Chen, L. W. A., Moosmüller, H., Arnott, W. P., Chow, J. C., Watson, J. G., Susott, R. A., et al. (2007). Emissions from laboratory combustion of wildland fuels: Emission factors and source profiles. Environmental Science & Technology, 41(12), 4317-4325.

Chylek, P., & Wong, J. (1995). Effect of absorbing aerosols on global radiation budget. Geophysical Research Letters, 22(8), 929-931.

Cinnirella, S., & Pirrone, N. (2006). Spatial and temporal distributions of mercury emissions from forest fires in Mediterranean region and Russian federation. Atmospheric Environment, 40(38), 7346-7361.

Dantonio, C. M., & Vitousek, P. M. (1992). Biological Invasions by Exotic Grasses, the Grass Fire Cycle, and Global Change. Annual Review of Ecology and Systematics, 23, 63-87.

Davies, K. W., & Nafus, A. M. (2013). Exotic annual grass invasion alters fuel amounts, continuity and moisture content. International Journal of Wildland Fire, 22(3), 353-358.

Engle, M. A., Gustin, M. S., Johnson, D. W., Murphy, J. F., Miller, W. W., Walker, R. F., et al. (2006). Mercury distribution in two Sierran forest and one desert sagebrush steppe ecosystems and the effects of fire. Science of the Total Environment, 367(1), 222-233.

Ericksen, J. A., Gustin, M. S., Schorran, D. E., Johnson, D. W., Lindberg, S. E., & Coleman, J. S. (2003). Accumulation of atmospheric mercury in forest foliage. Atmospheric Environment, 37(12), 1613-1622.

Finley, B. D., Swartzendruber, P. C., & Jaffe, D. A. (2009). Particulate mercury emissions in regional wildfire plumes observed at the Mount Bachelor Observatory. Atmospheric Environment, 43(38), 6074-6083.

Fitzgerald, W. F., & Gill, G. A. (1979). Sub-Nanogram Determination Of Mercury By 2-Stage Gold Amalgamation And Gas-Phase Detection Applied To Atmospheric Analysis. Analytical Chemistry, 51(11), 1714-1720.

Friedli, H. R., Arellano, A. F., Cinnirella, S., & Pirrone, N. (2009). Initial Estimates of Mercury Emissions to the Atmosphere from Global Biomass Burning. Environmental Science & Technology, 43(10), 3507-3513.

Friedli, H. R., Radke, L. F., Lu, J. Y., Banic, C. M., Leaitch, W. R., & MacPherson, J. I. (2003). Mercury emissions from burning of biomass from temperate North American forests: laboratory and airborne measurements. Atmospheric Environment, 37(2), 253-267.

Friedli, H. R., Radke, L. F., Prescott, R., Hobbs, P. V., & Sinha, P. (2003). Mercury emissions from the August 2001 wildfires in Washington State and an agricultural waste fire in Oregon and atmospheric mercury budget estimates. Global Biogeochemical Cycles, 17(2), 8.

Hassan, T., Moosmüller, H., & Chung, C. E. (2015). Coefficients of an analytical aerosol forcing equation determined with a Monte-Carlo radiation model. Journal of Quantitative Spectroscopy & Radiative Transfer, 164, 129-136.

Hopner, F., Bender, F. A. M., Ekman, A. M. L., Andersson, A., Gustafsson, O., & Leck, C. (2019). Investigation of Two Optical Methods for Aerosol-Type Classification Extended to a Northern Indian Ocean Site. Journal of Geophysical Research-Atmospheres, 124(15), 8743-8763.

Huang, X., Li, M. M., Friedli, H. R., Song, Y., Chang, D., & Zhu, L. (2011). Mercury Emissions from Biomass Burning in China. Environmental Science & Technology, 45(21), 9442-9448.

Lewis, K., Arnott, W. P., Moosmüller, H., & Wold, C. E. (2008). Strong spectral variation of biomass smoke light absorption and single scattering albedo observed with a novel dual-wavelength photoacoustic instrument. Journal of Geophysical Research-Atmospheres, 113(D16), 14.

Lyman, S. N., Gustin, M. S., Prestbo, E. M., & Marsik, F. J. (2007). Estimation of dry deposition of atmospheric mercury in Nevada by direct and indirect methods. Environmental Science & Technology, 41(6), 1970-1976.

Martinsson, J., Eriksson, A. C., Nielsen, I. E., Malmborg, V. B., Ahlberg, E., Andersen, C., et al. (2015). Impacts of Combustion Conditions and Photochemical Processing on the Light Absorption of Biomass Combustion Aerosol. Environmental Science & Technology, 49(24), 14663-14671.

McMeeking, G. R., Kreidenweis, S. M., Baker, S., Carrico, C. M., Chow, J. C., Collett, J. L., et al. (2009). Emissions of trace gases and aerosols during the open combustion of biomass in the laboratory. Journal of Geophysical Research-Atmospheres, 114, 20.

McMeeking, G. R., Kreidenweis, S. M., Baker, S., Carrico, C. M., Chow, J. C., Collett, J. L., et al. (2009). Emissions of trace gases and aerosols during the open combustion of biomass in the laboratory. Journal of Geophysical Research-Atmospheres, 114, 20.

Millhollen, A. G., Gustin, M. S., & Obrist, D. (2006). Foliar mercury accumulation and exchange for three tree species. Environmental Science & Technology, 40(19), 6001-6006.

Moosmüller, H., & Chakrabarty, R. K. (2011). Technical Note: Simple analytical relationships between Angstrom coefficients of aerosol extinction, scattering, absorption, and single scattering albedo. Atmospheric Chemistry and Physics, 11(20), 10677-10680.

Moosmüller , H., Chakrabarty, R. K., & Arnott, W. P. (2009). Aerosol light absorption and its measurement: A review. Journal of Quantitative Spectroscopy & Radiative Transfer, 110(11), 844-878.

Moosmüller, H., Chakrabarty, R. K., Ehlers, K. M., & Arnott, W. P. (2011). Absorption Angstrom coefficient, brown carbon, and aerosols: basic concepts, bulk matter, and spherical particles. Atmospheric Chemistry and Physics, 11(3), 1217-1225.

Moosmüller , H., Engelbrecht, J. P., Skiba, M., Frey, G., Chakrabarty, R. K., & Arnott, W. P. (2012). Single scattering albedo of fine mineral dust aerosols controlled by iron concentration. Journal of Geophysical Research-Atmospheres, 117, 10.

Moosmüller, H., & Sorensen, C. M. (2018a). Single scattering albedo of homogeneous, spherical particles in the transition regime. Journal of Quantitative Spectroscopy & Radiative Transfer, 219, 333-338.

Moosmüller, H., & Sorensen, C. M. (2018b). Small and large particle limits of single scattering albedo for homogeneous, spherical particles. Journal of Quantitative Spectroscopy & Radiative Transfer, 204, 250-255.

Niu, Z. C., Zhang, X. S., Wang, Z. W., & Ci, Z. J. (2011). Field controlled experiments of mercury accumulation in crops from air and soil. Environmental Pollution, 159(10), 2684-2689.

Obrist, D., Moosmuller, H., Schurmann, R., Chen, L. W. A., & Kreidenweis, S. M. (2008). Particulate-phase and gaseous elemental mercury emissions during biomass combustion: Controlling factors and correlation with particulate matter emissions. Environmental Science & Technology, 42(3), 721-727.

Obrist, D., Moosmüller, H., Schurmann, R., Chen, L. W. A., & Kreidenweis, S. M. (2008). Particulate-phase and gaseous elemental mercury emissions during biomass combustion: Controlling factors and correlation with particulate matter emissions. Environmental Science & Technology, 42(3), 721-727.

Pistone, K., Redemann, J., Doherty, S., Zuidema, P., Burton, S., Cairns, B., et al. (2019). Intercomparison of biomass burning aerosol optical properties from in situ and remote-sensing instruments in ORACLES-2016. Atmospheric Chemistry and Physics, 19(14), 9181-9208.

Rea, A. W., Lindberg, S. E., Scherbatskoy, T., & Keeler, G. J. (2002). Mercury accumulation in foliage over time in two northern mixed-hardwood forests. Water Air and Soil Pollution, 133(1-4), 49-67.

Rein, G. u. (2016). Smoldering Combustion. In H. M. J. e. al. (Ed.), SFPE Handbook of Fire Protection Engineering (pp. pp 581-603). New York, NY: Springer, New York, NY.

Rutter, A. P., Schauer, J. J., Shafer, M. M., Creswell, J. E., Olson, M. R., Robinson, M., et al. (2011). Dry deposition of gaseous elemental mercury to plants and soils using mercury stable isotopes in a controlled environment. Atmospheric Environment, 45(4), 848-855.

Samburova, V., Connolly, J., Gyawali, M., Yatavelli, R. L. N., Watts, A. C., Chakrabarty, R. K., et al. (2016). Polycyclic aromatic hydrocarbons in biomass-burning emissions and their contribution to light absorption and aerosol toxicity. Science of the Total Environment, 568, 391-401.

Satheesh, S. K., & Moorthy, K. K. (2005). Radiative effects of natural aerosols: A review. Atmospheric Environment, 39(11), 2089-2110.

Schroeder, W. H., & Munthe, J. (1998). Atmospheric mercury - An overview. Atmospheric Environment, 32(5), 809-822.

Selimovic, V., Yokelson, R. J., Warneke, C., Roberts, J. M., de Gouw, J., Reardon, J., et al. (2018). Aerosol optical properties and trace gas emissions by PAX and OP-FTIR for laboratory-simulated western US wildfires during FIREX. Atmospheric Chemistry and Physics, 18(4), 2929-2948.

Seo, Y. S., Jeong, S. P., Holsen, T. M., Han, Y. J., Choi, E., Park, E. H., et al. (2016). Characteristics of total gaseous mercury (TGM) concentrations in an industrial complex in South Korea: impacts from local sources. Atmospheric Chemistry and Physics, 16(15), 10215-10228.

Stocks, B. J., Fosberg, M. A., Lynham, T. J., Mearns, L., Wotton, B. M., Yang, Q., et al. (1998). Climate change and forest fire potential in Russian and Canadian boreal forests. Climatic Change, 38(1), 1-13.

Streets, D. G., Hao, J. M., Wu, Y., Jiang, J. K., Chan, M., Tian, H. Z., et al. (2005). Anthropogenic mercury emissions in China. Atmospheric Environment, 39(40), 7789-7806.

Tian, J., Chow, J. C., Cao, J. J., Han, Y., Ni, H. Y., Chen, L. W. A., et al. (2015). A Biomass Combustion Chamber: Design, Evaluation, and a Case Study of Wheat Straw Combustion Emission Tests. Aerosol and Air Quality Research, 15(5), 2104-2114.

Urbanski, S. (2014). Wildland fire emissions, carbon, and climate: Emission factors. Forest Ecology and Management, 317, 51-60.

Urbanski, S. P. (2013). Combustion efficiency and emission factors for wildfire-season fires in mixed conifer forests of the northern Rocky Mountains, US. Atmospheric Chemistry and Physics, 13(14), 7241-7262.

Urbanski, S. P., Reeves, M. C., Corley, R. E., Silverstein, R. P., & Hao, W. M. (2018). Contiguous United States wildland fire emission estimates during 2003-2015. Earth System Science Data, 10(4), 2241-2274.

Wiedinmyer, C., & Friedli, H. (2007). Mercury emission estimates from fires: An initial inventory for the United States. Environmental Science & Technology, 41(23), 8092-8098.

Zhou, Y., Xing, X. F., Lang, J. L., Chen, D. S., Cheng, S. Y., Wei, L., et al. (2017). A comprehensive biomass burning emission inventory with high spatial and temporal resolution in China. Atmospheric Chemistry and Physics, 17(4), 2839-2864.

Conclusions

Cheatgrass is greatly affecting the ecosystem wildland fires will continue to become more frequent and intense while cheatgrass continues to invade the Great Basin. Here, we presented measurements of the optical and combustion properties of smoke emitted in the open combustion of cheatgrass laboratory burns. Cheatgrass modified combustion properties reported here are comparable to prescribed fire grassland, Dambo Grass, Montana Grass, and Savanna and grasslands modified combustion efficiency. Comparison of the EF_{CO2}, EF_{CO}, and EF_{PM} reported for our monthly fuel burn, EFs from the campaign in 2014 are in good agreement with other previously reported EF_{CO2}, EF_{CO}, and EF_{PM} for prescribed fire grassland, Dambo grass, Montana grass, and grasslands and savannahs and contribute to regional emissions of greenhouse gases during wildland fires.

The gaseous elemental mercury emission factors of cheatgrass reported here are in quantitative agreement with the EFs for South African savanna that has been previously published in literature. Cheatgrass EF_{GEM} are mostly lower than those in previously published literature for EF_{GEM} from wildland fire plumes. While mercury emission factors measured in the combustion chamber for cheatgrass are small compared to EFs of wildfire plumes from grassland fire in the Mediterranean, grass stems, grass leaves, and open shrublands, they should be taken into consideration when evaluating the future transport of Hg from biomass burning. As cheatgrass continues to invade the sagebrush ecosystem, characterization of emission factors and optical properties of the smoke from cheatgrass wildland fires offer a better understanding of the effect cheatgrass combustion has on changing the regional energy budget and greenhouse gas emissions.